RESEARCH BRIEF

Jak2^{V617F} Reversible Activation Shows Its Essential Requirement in Myeloproliferative Neoplasms

Andrew J. Dunbar[1,2,3], Robert L. Bowman[1], Young C. Park[1], Kavi O'Connor[1], Franco Izzo[4,5], Robert M. Myers[4,5], Abdul Karzai[1], Zachary Zaroogian[1], Won Jun Kim[1], Inés Fernández-Maestre[1,6], Michael R. Waarts[1,6], Abbas Nazir[1], Wenbin Xiao[1,7], Tamara Codilupi[8], Max Brodsky[1,9], Mirko Farina[1,10], Louise Cai[1], Sheng F. Cai[1,2], Benjamin Wang[1], Wenbin An[11], Julie L. Yang[12], Shoron Mowla[1], Shira E. Eisman[1], Amritha Varshini Hanasoge Somasundara[1], Jacob L. Glass[1,2,12], Tanmay Mishra[1], Remie Houston[1], Emily Guzzardi[1], Anthony R. Martinez Benitez[1], Aaron D. Viny[13], Richard P. Koche[12], Sara C. Meyer[8,14], Dan A. Landau[4,5], and Ross L. Levine[1,2,3,12]

ABSTRACT

Gain-of-function mutations activating JAK/STAT signaling are seen in the majority of patients with myeloproliferative neoplasms (MPN), most commonly *JAK2*^{V617F}. Although clinically approved JAK inhibitors improve symptoms and outcomes in MPNs, remissions are rare, and mutant allele burden does not substantively change with chronic therapy. We hypothesized this is due to limitations of current JAK inhibitors to potently and specifically abrogate mutant JAK2 signaling. We therefore developed a conditionally inducible mouse model allowing for sequential activation, and then inactivation, of *Jak2*^{V617F} from its endogenous locus using a combined Dre-*rox*/Cre-*lox* dual-recombinase system. *Jak2*^{V617F} deletion abrogates MPN features, induces depletion of mutant-specific hematopoietic stem/progenitor cells, and extends overall survival to an extent not observed with pharmacologic JAK inhibition, including when cooccurring with somatic *Tet2* loss. Our data suggest JAK2^{V617F} represents the best therapeutic target in MPNs and demonstrate the therapeutic relevance of a dual-recombinase system to assess mutant-specific oncogenic dependencies *in vivo*.

SIGNIFICANCE: Current JAK inhibitors to treat myeloproliferative neoplasms are ineffective at eradicating mutant cells. We developed an endogenously expressed *Jak2*^{V617F} dual-recombinase knock-in/knock-out model to investigate *Jak2*^{V617F} oncogenic reversion *in vivo*. *Jak2*^{V617F} deletion abrogates MPN features and depletes disease-sustaining MPN stem cells, suggesting improved JAK2^{V617F} targeting offers the potential for greater therapeutic efficacy.

See related commentary by Celik and Challen, p. 701.

[1]Human Oncology & Pathogenesis Program, Memorial Sloan Kettering Cancer Center, New York, New York. [2]Leukemia Service, Department of Medicine and Center for Hematologic Malignancies, Memorial Sloan Kettering Cancer Center, New York, New York. [3]Myeloproliferative Neoplasm-Research Consortium. [4]Weill Cornell Medical College of Cornell University, New York, New York. [5]New York Genome Center, New York, New York. [6]Louis V. Gerstner Jr Graduate School of Biomedical Sciences, Memorial Sloan Kettering Cancer Center, New York, New York. [7]Department of Pathology, Memorial Sloan Kettering Cancer Center, New York, New York. [8]Department of Biomedicine, University of Basel, Basel, Switzerland. [9]Department of Medicine, Johns Hopkins University School of Medicine, Baltimore, Maryland. [10]Unit of Blood Diseases and Bone Marrow Transplantation, Cell Therapies and Hematology Research Program, University of Brescia, ASST Spedali Civili di Brescia, Italy. [11]State Key Laboratory of Experimental Hematology, National Clinical Research Center for Blood Diseases, Institute of Hematology & Blood Diseases Hospital, Chinese Academy of Medical Sciences & Peking Union Medical College, Tianjin, China. [12]Center for Epigenetics Research, Memorial Sloan Kettering Cancer Center, New York, New York. [13]Division of Hematology and Oncology, Department of Medicine and Columbia Stem Cell Initiative, Columbia University Irving Medical Center, New York, New York. [14]Department of Hematology and Central Hematology Laboratory, Inselspital, Bern University Hospital, University of Bern, Bern, Switzerland.

A.J. Dunbar and R.L. Bowman contributed equally to this article.

Corresponding Author: Ross L. Levine, Memorial Sloan Kettering Cancer Center, 1275 York Avenue, Box 20, New York, NY 10065. E-mail: leviner@mskcc.org

Cancer Discov 2024;14:737–51

doi: 10.1158/2159-8290.CD-22-0952

INTRODUCTION

Somatic mutations that constitutively activate JAK2 signaling are seen in the majority of patients with myeloproliferative neoplasm (MPN) (1), most commonly the recurrent *JAK2*^{V617F} alteration, and murine models suggest a critical role for JAK/STAT pathway mutations in promoting the MPN phenotype *in vivo* (2–6). In contrast to ABL1 kinase inhibition in BCR-ABL1–driven chronic myelogenous leukemia (7), current JAK inhibitors fail to reduce mutant clonal fraction and do not induce pathologic regression of key disease features including myeloproliferation and bone marrow fibrosis, and most patients lose their response over time (8, 9). To date, second-site *JAK2* mutations have not been observed as a mechanism of acquired resistance (10), and different mechanisms have been postulated to mediate the inadequate efficacy of JAK inhibition, including incomplete dependency on JAK2 signaling and the presence of cooccurring mutant disease alleles (11). We hypothesized that the limited potency of JAK inhibition relates to insufficient mutant kinase inhibition at achievable therapeutic doses (4, 12), and we and others have elucidated mechanisms by which mutant JAK2 can signal in the presence of type I JAK inhibitors (12–14). Previous model systems evaluating doxycycline-inducible *Jak2*^{V617F} expression highlight the importance of oncogenic JAK2^{V617F} signaling in sustaining the MPN phenotype (6); however, these systems were limited by the inability to accurately recapitulate reversal of endogenous mutant expression or allow for assessment of oncogenic dependency on MPN hematopoietic stem cell (HSC) fitness alone or in context of comutations acquired during clonal evolution and myeloid transformation. Given this, we developed a system that would more definitively assess JAK2^{V617F} dependency in MPN.

RESULTS

A Conditional Knock-in, Knock-Out Model of *Jak2*^{V617F} MPN

To assess the requirement for JAK2^{V617F} oncogenic signaling in MPN disease maintenance, we generated a Dre-*rox* (15), Cre-*lox* (16) dual-recombinase *Jak2*^{V617F} knock-in/knock-out mouse model (*Jak2*$^{Rox/Lox}$/*Jak2*^{RL}) by gene targeting in mouse embryonic stem cells (Fig. 1A). The close proximity of the *lox* sites (82 base pairs) prevents Cre-mediated deletion prior to Dre-mediated recombination and *Jak2*^{V617F} induction. Once the mutant allele is activated, the *lox* sites separate allowing for subsequent Cre-mediated deletion of *Jak2*^{V617F}, including models in which cooperating alleles are induced by antecedent Cre-mediated activation/deletion. A similar strategy, which we have termed GOLDI-Lox for governing oncogenic loci by Dre inversion and *lox* deletion, was also used to target *Flt3*^{ITD} (17). Given previous literature demonstrating that *Jak2* expression is essential for hematopoiesis (18, 19), all *Jak2*^{RL} mice used for experiments were heterozygous, with one maintained copy of the wild-type (WT) *Jak2* allele (Supplementary Fig. S1A). In the absence of Dre recombination, *Jak2*$^{RL/+}$ heterozygous mice displayed no observable phenotype, consistent with previous studies (not shown; refs. 2, 18–21). Sequencing of the *Jak2*^{RL} locus on sorted Cre reporter cells (22) after Cre recombinase exposure confirmed retainment of the nonrecombined *Jak2*^{RL} locus (Supplementary Fig. S1B). We transiently expressed Dre recombinase by mRNA electroporation *ex vivo* in primary lineage-negative bone marrow cells, efficiently inducing *Jak2*^{V617F} activation and separation of *lox* sites by inversion (Supplementary Fig. S1C). Single-colony genotyping of these cells cultured in methylcellulose for 7 days revealed evidence of knock-in in 28%–55% of assayed colonies ($n = 33$/replicate). Efficient *Jak2*^{V617F}-mutant induction was also observed in lineage-negative bone marrow harvested from primary transplant donors 6 weeks following electroporation and transplant (Supplementary Fig. S1D and S1E). By 3 weeks posttransplant, lethally irradiated mice transplanted with Dre-inducible *Jak2*^{RL} knock-in bone marrow developed a highly penetrant and fully transplantable MPN characterized by leukocytosis with myeloid preponderance, elevated hematocrit with erythroid progenitor expansion in bone marrow, hepatosplenomegaly, and megakaryocytic hyperplasia consistent with prior *Jak2*^{V617F} conditional knock-in mouse models of MPN (Supplementary Fig. S1F–S1J; ref. 3). Variable bone marrow fibrosis was observed across primary and secondary transplant recipient cohorts. Although there was minimal evidence of fibrosis in primary recipient mice, in secondarily transplanted mice, by >16 weeks, we observed 0–2+ reticulin fibrosis in 14 of 23 (61%) mice across multiple independent noncompetitive and competitive transplant studies ($n = 5$; Supplementary Fig. S1K).

To assess the reversibility of the *Jak2*^{RL} construct, we cultured *Dre*-electroporated, lineage-negative, tamoxifen-inducible *Ubc:CreER-Jak2*^{RL} cells isolated from donor mice with active MPN *ex vivo* with increasing doses of 4-hydroxytamoxifen (4-OHT) over bone marrow endothelial cells (BMEC; Supplementary Fig. S2A; ref. 23). Treatment with 4-OHT resulted in deletion of the *Jak2*^{V617F} allele, which was confirmed by excision PCR (Supplementary Fig. S2B). Loss of *Jak2*^{V617F} significantly reduced cell numbers *ex vivo* (mean 4-OHT 0.18×10^6/mL vs. vehicle 2.19×10^6/mL, $P \leq 0.0001$), including within immunophenotypically defined hematopoietic stem/progenitor cell (HSPC) compartments, a phenotypic change not observed with vehicle-treated *Jak2*^{RL}, Cre-inducible *Jak2*^{V617F} (*Jak2*^{Crelox}; $P \leq 0.228$; ref. 2), or Cre-inducible WT cells ($P \leq 0.114$; Supplementary Fig. S2C–S2G). Loss of *Jak2*^{V617F} also abrogated erythropoietin-independent erythroid differentiation (24) *in vitro* ($P \leq 0.01$; Supplementary Fig. S2H). The cell loss observed was associated with enhanced apoptosis, which was most apparent in Mac1$^+$ mature myeloid cells (mean 4-OHT 35% vs. vehicle 9.3%, $P \leq 0.005$; Supplementary Fig. S2I).

We next evaluated the impact of reversible *Jak2*^{V617F} expression *in vivo*. Twelve weeks posttransplant, secondary recipient mice transplanted with *Dre*-electroporated *Ubc:CreER-Jak2*^{RL} whole bone marrow and exhibiting MPN were administered tamoxifen to delete *Jak2*^{V617F} (Supplementary Fig. S3A). A sequential *rox*-stop-*rox*, *lox*-TdTomato-stop-*lox*-eGFP dual-recombinase reporter system (25), in which TdTomato is expressed following Dre and then TdTomato deletion with concomitant GFP$^+$ induction is expressed following Cre, was used to validate *Jak2*^{V617F}

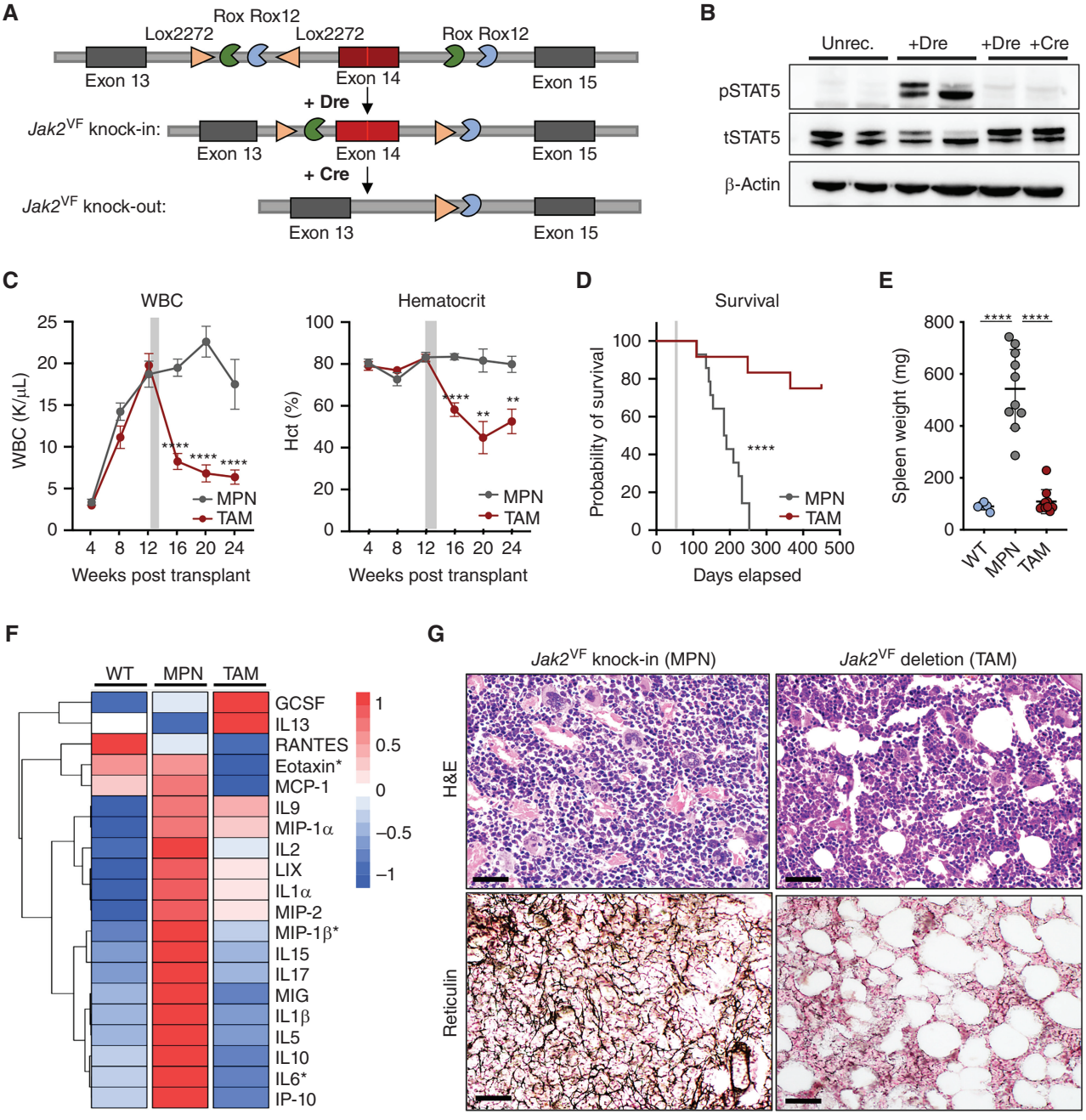

Figure 1. *Jak2*^{V617F} deletion abolishes JAK/STAT signaling and abrogates the MPN phenotype. **A,** Schematic representation of the dual-recombinase *Jak2*^{V617F} conditional knock-in/knock-out allele (*Jak2*^{RL}), the *Jak2*^{RL} knock-in allele following Dre recombination, and the null recombined allele following Cre-mediated deletion. Semicircles indicate *Rox* sequences; triangles indicate *lox*P sequences. **B,** Representative Western blot depicting phospho-STAT5 abundance of Dre-mediated *Jak2*^{V617F} knock-in (+Dre) vs. *Jak2*^{V617F}-deleted (+Dre +Cre) states from isolated splenocytes 7 days following tamoxifen (TAM) administration in comparison with unrecombined (Unrec.) *Jak2*^{RL} cells ($n = 2$ biological replicates each; representative of $n = 2$ independent experiments). **C,** Peripheral blood count trends (weeks 0–24) of MPN vs. tamoxifen (*Jak2*^{V617F}-deleted) treated mice: WBCs (left), Hct (right; $n \geq 10$ per arm; mean ± SEM). Gray bar represents duration of tamoxifen pulse/chow administration. Representative of $n = 2$ independent transplants. **, $P \leq 0.01$; ****, $P \leq 0.0001$. **D,** Kaplan–Meier survival analysis of MPN vs. tamoxifen (*Jak2*^{V617F}-deleted) treated mice ($n \geq 12$ per arm; log-rank test). Gray bar represents duration of tamoxifen pulse/chow administration. ****, $P \leq 0.0001$. **E,** Spleen weights of MPN vs. tamoxifen (*Jak2*^{V617F}-deleted) treated mice at timed sacrifice (24 weeks) in comparison with WT control mice (mean ± SEM). Representative of $n = 2$ independent transplants. ****, $P \leq 0.0001$. **F,** Heat map scaled using Z-scores of serum cytokine/chemokine concentrations of MPN vs. tamoxifen (*Jak2*^{V617F}-deleted) treated mice harvested at time of sacrifice 18–24 weeks posttransplant in comparison with WT control mice ($n = 4$–7 biological replicates per arm pooled from $n = 3$ transplants). Asterisks denote cytokines with FDR ≤ 0.05. Kruskal–Wallis test with FDR correction. **G,** Representative hematoxylin and eosin (H&E) and reticulin stains of bone marrow of MPN (Control) vs. tamoxifen (*Jak2*^{V617F}-deleted) treated mice from timed sacrifice at 24 weeks. Representative micrographs of $n = 6$ individual mouse replicates per arm. All images represented at 400× magnification. Scale bar, 20 μm.

deletion within Cd45.2 reporter–positive cell populations (Supplementary Fig. S3B). Deletion of *Jak2*^{V617F} was also validated *in vivo* at the transcriptional level ($P \leq 0.0001$; Supplementary Fig. S3C) and was associated with loss of constitutive JAK/STAT signaling (Fig. 1B). Consistent with our *in vitro* data, we observed normalization of white blood cell (WBC; mean tamoxifen 6.18 K/μL vs. MPN 17.5 K/μL, $P \leq 0.0001$), hematocrit (Hct; mean 52.6% vs. 79.9%, $P \leq 0.01$), and platelet (mean 786 K/μL vs. 2146 K/μL, $P \leq 0.0004$) parameters within 4 weeks following tamoxifen treatment that persisted until timed sacrifice at 24 weeks (Fig. 1C; Supplementary Fig. S3D). As early as 7 days post-tamoxifen, we observed an increase in Annexin V$^+$ cells (mean tamoxifen 34.1% vs. MPN 8.4%, $P \leq 0.01$) in HSPC fractions consistent with an acute induction of apoptosis and concomitant reduction in the percentage of cycling HSPCs by flow (G_2–M phase tamoxifen 9.4% vs. MPN 14.9%, $P \leq 0.01$; Supplementary Fig. S3E and S3F). Two of 12 mice demonstrated reemergence/persistence of the MPN phenotype, both of which showed incomplete excision of the *Jak2*^{RL} allele highlighting the necessity of JAK2^{V617F} in disease maintenance (Supplementary Fig. S3G). WT *Jak2* mRNA levels were increased at 7 days following oncogenic reversion, an effect that was sustained at the protein level until timed sacrifice at 24 weeks, as evidenced by Western blot analysis of harvested splenocytes, suggesting a potential compensatory mechanism in response to oncogenic reversion (Supplementary Fig. S3H and S3I). Genetic reversal of *Jak2*^{V617F} significantly prolonged overall survival (median not defined vs. 187 days, $P \leq 0.0012$) and led to loss of disease-defining MPN features in the majority of mice (9/12; Fig. 1D). Spleen weights (mean 108.9 mg vs. 542.7 mg, $P \leq 0.0001$) were reduced, and we observed an overall trend in reduction of multiple inflammatory cytokines with *Jak2*^{V617F} reversal (Fig. 1E and F). Significant cytokine reductions, although similar to what has previously been seen in patient samples receiving ruxolitinib therapy (26, 27), including IL6 (FDR ≤ 0.015) and MIP-1β (FDR ≤ 0.018), also showed reductions in serum Eotaxin (FDR ≤ 0.024) at time of sacrifice and a trend toward reduction with IP-10 (FDR ≤ 0.067; Supplementary Fig. S3J). Histopathologic analysis of bone marrow and spleen revealed reductions in megakaryocytic hyperplasia, splenic infiltration, reduced overall cellularity, and absence of bone marrow and spleen fibrosis in 8 of 9 assayed *Jak2*^{V617F}-deleted mice that persisted until timed sacrifice at 24 weeks (Fig. 1G; Supplementary Fig. S3K). The phenotypes observed with *Ubc:CreER-Jak2*^{V617F} deletion *in vivo*, including the histologic effects, were not observed with tamoxifen administration in the absence of *Jak2*^{V617F} reversal (Supplementary Fig. S4A–S4G). We conclude that the MPN phenotype requires maintenance of oncogenic signaling through JAK2^{V617F}.

Jak2^{V617F} Reversal Impairs the Fitness of MPN Cells, Including MPN HSCs

We next evaluated *Dre*-electroporated *Jak2*^{RL} bone marrow from Cd45.2 MPN donors in competition with Cd45.1 competitor cells to explore effects of *Jak2*^{V617F} deletion on peripheral blood and bone marrow–mutant cell fitness (Supplementary Fig. S5A). Both early (3 weeks posttransplant) or late (12 weeks) administration of tamoxifen resulted in abrupt, durable reductions in Cd45.2-mutant cell fraction in the peripheral blood (mean 24.5% vs. 63.9%, $P \leq 0.001$), coinciding with normalization of hematologic parameters that persisted until the time of sacrifice (Fig. 2A; Supplementary Fig. S5B). Consistent with the *in vitro* data, this effect was most pronounced in Mac1$^+$ myeloid cell fractions ($P \leq 0.0001$; Supplementary Fig. S5C). In bone marrow at timed sacrifice (24 weeks), the reductions in mutant cell fraction among the different HSPC compartments were more significant than those observed in peripheral blood, including within megakaryocytic-erythroid progenitor (MEP; Lineage$^-$cKit$^+$Sca1$^-$Cd34$^-$Fcg$^-$; $P \leq 0.0001$) and granulocytic-monocytic progenitor (GMP; Lineage$^-$cKit$^+$Sca1$^-$Cd34$^+$Fcg$^+$; $P \leq 0.0001$) populations and most importantly the LSK (Lineage$^-$cKit$^+$Sca1$^+$; $P \leq 0.0096$) stem cell compartment, including the SLAM-positive LSK population enriched for long-term HSCs (LT-HSC; Lineage$^-$Sca1$^+$cKit$^+$Cd150$^+$Cd48$^-$; $P \leq 0.01$; Fig. 2B; Supplementary Fig. S5D–S5F). Similar reductions in mutant cell fraction as well as reductions in Ter119$^+$Cd71$^+$ erythroid precursors were also observed in whole spleen ($P \leq 0.05$) in both early- and late-tamoxifen cohorts consistent with an attenuation of extramedullary hematopoiesis (Supplementary Fig. S5G and S5H). Recurrent MPN, as was seen in the noncompetitive setting, was observed in 3 of 14 mice across both early- and late-treatment arms and corresponded with residual mutant *Jak2*^{V617F} expression and sustained mutant chimerism at sacrifice. We next queried mice without MPN, but persistent Cd45.2$^+$ cells from this transplant. In 8 of 8 mice assayed, we observed neither *Jak2*^{V617F} knock-in nor *Jak2*^{V617F} excision bands by PCR on sorted Cd45.2$^+$ LSK cells (n = 3 early tamoxifen, n = 5 late tamoxifen), suggesting residual Cd45.2$^+$ cells in these mice represent a non-Dre recombined *Jak2*^{RL} WT bystander cell population. Similar results were observed in a separate competitive transplant study; however, in 1 of 8 late tamoxifen-treated mice, we also observed a faint knock-in band despite no phenotypic evidence of MPN, suggesting that in a minority of mice, residual mutant cells can remain and not necessarily give rise to disease (Supplementary Fig. S5I). Transplant of unfractionated *Jak2*^{RL}-deleted bone marrow failed to form phenotypic disease in 4 of 5 secondary transplant recipient mice consistent with depletion of disease-propagating MPN HSCs (Supplementary Fig. S5J–S5L).

We sought to characterize transcriptional changes following acute *Jak2*^{V617F} reversal. We performed RNA sequencing (RNA-seq) analysis of purified HSPCs 3 and 7 days following *Jak2*^{V617F} deletion (n = 3–4) compared with MPN controls (n = 3–4). Transcriptional analysis of sorted, *Jak2*^{V617F}-deleted LSK and MEP populations revealed near-complete loss of expression of STAT5 target genes as early as 3 days post-deletion [LSK: normalized enrichment score (NES) = −1.77, FDR ≤ 0.002; MEP: NES = −1.53, FDR ≤ 0.0065] indicating immediate disengagement from disease-defining pathway signaling (Supplementary Fig. S6A). By 7 days, we observed significant negative enrichment in IFNγ (NES = −1.61, FDR ≤ 0.0005), TGFβ (NES = −1.45, FDR ≤ 0.071), and TNFα via NFκB (NES = −1.54, FDR ≤ 0.0017) Hallmark proinflammatory response pathways as well as downregulation of MAPK (NES = −1.52, FDR ≤ 0.0052) and MTORC1 (NES = −1.46,

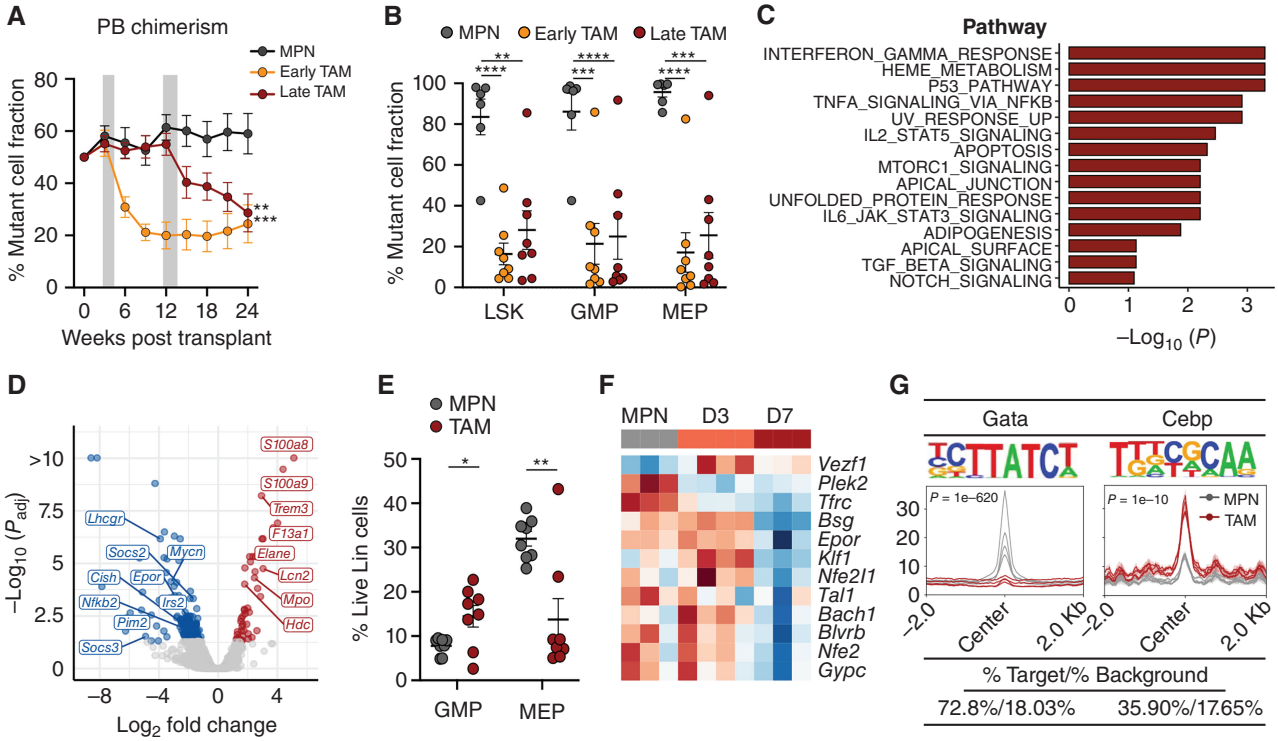

Figure 2. *Jak2*^{V617F} reversal impairs the fitness of MPN cells, including MPN stem cells. **A,** Peripheral blood (PB) mutant Cd45.2 percent chimerism trend (weeks 0–24) of early (3 weeks posttransplant) tamoxifen (TAM; *Jak2*^{V617F}-deleted) treated (gold bar) and late (12 weeks posttransplant) tamoxifen-treated (maroon bar) mice ($n = 8$ each) in comparison with MPN (dark gray bar; $n = 6$) mice (mean ± SEM). Gray bars represent duration of tamoxifen pulse/chow administration. Representative of $n = 2$ independent transplants. **, $P \leq 0.01$; ***, $P \leq 0.001$. **B,** Bone marrow–mutant cell fraction within LSK (Lineage$^-$Sca1$^+$cKit$^+$), granulocytic-monocytic progenitor (GMP; Lineage$^-$cKit$^+$Sca1$^-$Cd34$^+$Fcg$^+$), and megakaryocytic-erythroid progenitor (MEP; Lineage$^-$cKit$^+$Sca1$^-$Cd34$^-$Fcg$^-$) compartments of early (3 weeks posttransplant) tamoxifen (*Jak2*^{V617F}-deleted) treated and late (12 weeks posttransplant) tamoxifen-treated mice in comparison with MPN mice at timed sacrifice of 24 weeks ($n = 6$–8 individual biological replicates per arm; mean ± SEM). Representative of $n = 2$ independent transplants. **, $P \leq 0.01$; ***, $P \leq 0.001$; ****, $P \leq 0.0001$. **C,** Gene-set enrichment analysis (GSEA) of significant Hallmark gene sets of MPN vs. tamoxifen (*Jak2*^{V617F}-deleted) treated LSKs isolated 7 days after initiation of tamoxifen ($n = 3$–4 biological replicates per arm). **D,** Volcano plot demonstrating differential gene expression of MPN vs. tamoxifen (*Jak2*^{V617F}-deleted) treated LSKs 7 days following initiation of tamoxifen ($n = 3$–4 biological replicates per arm). **E,** GMP and MEP stem cell frequencies of MPN vs. tamoxifen (*Jak2*^{V617F}-deleted) treated mice 7 days following initiation of tamoxifen ($n = 8$ biological replicates per arm across two independent transplants; mean ± SEM). **F,** Row normalized heat map of RNA-seq data of key erythroid differentiation factor genes from harvested MEPs at baseline (MPN), day 3 (D3), and day 7 (D7) following initiation of tamoxifen (*Jak2*^{V617F} deletion). **G,** HOMER motif analysis from ATAC-seq data demonstrating decreased accessibility of Gata motif signatures with concomitant increased accessibility of Cebp motif signatures of tamoxifen-treated (*Jak2*^{V617F}-deleted) cKit$^+$ bone marrow cells isolated 7 days following initiation of treatment in comparison with MPN cells ($n = 3$ biological replicates per arm). Non-Sig., nonsignificant.

FDR ≤ 0.0071) targets in LSKs, suggesting abrupt reduction in proinflammatory and proliferative signaling in the setting of *Jak2*^{V617F} deletion (Fig. 2C; Supplementary Fig. S6B; Supplementary Table S1). A flux toward increased expression of myeloid genes sets compared to erythroid gene sets was also observed at 7 days post-tamoxifen initiation, characterized by increased *S100a8*, *S100a9*, *Mpo*, and *Hdc* expression in LSKs; increases in GMP (mean 14.5% vs. 7.8%, $P \leq 0.018$) versus MEP (mean 13.8% vs. 32%, $P \leq 0.0025$) frequencies within the HSPC compartment; and enrichment in bone marrow Mac1$^+$ myeloid cells (mean 41.7% vs. 27.8%, $P \leq 0.0084$; Fig. 2D and E; Supplementary Fig. S6C). In line with reduced erythroid output, we also observed a marked decrease in heme metabolism in MEPs (NES = –2.07, FDR ≤ 4.71×10^{-5}) with associated reductions in critical erythroid/megakaryocytic transcription factors and signaling mediators, including *Nfe2* (28), *Plek2* (29), and *EpoR* (30), which coincided with concomitant reductions in total erythroid progenitor cell numbers ($P \leq 0.021$) and significantly reduced burst-forming unit-erythroid (BFU-E) colony output of *Jak2*^{V617F}-deleted cells ($P \leq 0.001$; Fig. 2F; Supplementary Fig. S6D–S6F). Assay for Transposase Accessible Chromatin with high-throughput sequencing (ATAC-Seq) on *Jak2*^{V617F}-deleted cKit$^+$ cells demonstrated an increase in open chromatin with Cebp motifs ($P \leq 1 \times 10^{-10}$) and reduced accessibility at GATA motifs ($p \leq 1 \times 10^{-620}$), including at critical erythroid loci (e.g., *EpoR*; $\log_2$FC = 1.49, FDR ≤ 0.00135), further consistent with an erythroid-to-myeloid lineage switch (Fig. 2G; Supplementary Fig. S6G; Supplementary Table S2). Lineage deconvolution (31) further suggested priming of cKit$^+$ cells toward a monocyte-to-granulocyte maturation switch in the setting of oncogenic reversion, consistent with our flow cytometric data showing changes in lineage output before and after mutational reversion (Supplementary Fig. S6H). Although reduced accessibility at putative GATA target sites was observed, we did not observe differential expression of either *Gata1* ($P \leq 1.0$) or *Gata2* ($P \leq 0.82$) in *Jak2*^{V617F}-deleted LSKs or MEPs compared with controls. These data suggest the transcriptional networks regulating the MPN phenotype

are not obligated to be achieved through transcription factor expression dysregulation but through differential transcription factor–mediated output.

Differential Efficacy of *Jak2*^{V617F} Deletion Compared with JAK Inhibitor Therapy

Given the limited ability of current JAK inhibitors to achieve disease modification and/or clonal remissions in polycythemia vera and myelofibrosis, we next compared the phenotypic and transcriptional effects of JAK inhibitor therapy with ruxolitinib to the effects of *Jak2*^{V617F} reversal. We first performed RNA-seq on *Jak2*^{V617F}-mutant LSKs and MEPs following 7 days of ruxolitinib treatment ($n = 3$) and compared this to the effects of *Jak2*^{V617F} deletion ($n = 3$). JAK-STAT target gene expression and erythroid pathway gene expression were much less potently inhibited with ruxolitinib than with *Jak2*^{V617F} deletion. Specifically, *Jak2*^{V617F} deletion resulted in a significant reduction in JAK/STAT signaling (NES = −1.51, $P \leq 0.003$) and expression of negative regulators including *Socs2* (32), *Pim2* (33), and *Cish* (34). In contrast, ruxolitinib treatment was associated with a muted reduction in the same targets, with no significant changes in STAT5 target gene expression identified by GSEA (NES = −0.913, $P = 0.84$) at this time point (Fig. 3A; Supplementary Fig. S7A; Supplementary Table S3). Furthermore, the alterations in erythroid pathway gene expression in MEPs (NES = 1.45, $P \leq 0.012$ vs. NES = −1.82, $P \leq 0.0005$) and skewing of GMP and MEP frequencies observed with *Jak2*^{V617F} deletion were not observed with ruxolitinib (mean GMP: vehicle 6.93% vs. ruxolitinib 6.66% vs. tamoxifen 20.1%, $P = 0.91$ vs. $P \leq 0.0001$, MEP: vehicle 27.1% vs. ruxolitinib 35.3% vs. tamoxifen 14.2%, $P = 0.25$ vs. $P = 0.014$; Fig. 3B and C; Supplementary Fig. S7B and S7C). Expression of the gene sets associated with TGFβ ($P = 0.65$) and TNFα/NFκB ($P = 0.90$) inflammatory signaling pathways also displayed minimal changes with ruxolitinib and were more potently downregulated with *Jak2*^{V617F} deletion. Consistent with this lack of change, genotype-aware single-cell ATAC-seq (scATAC-seq) on myelofibrosis patient samples (Supplementary Table S4) demonstrated unaltered NFκB accessibility in *JAK2*^{V617F}-mutant HSPCs following JAK inhibitor treatment (Fig. 3D; Supplementary Fig. S7D; see Myers and colleagues (35) supporting the notion of insufficient mitigation of inflammatory signaling by JAK inhibition on MPN-sustaining stem cells.

To evaluate the phenotypic effects of *Jak2*^{V617F} deletion in direct comparison to JAK kinase inhibition, we performed an *in vivo* trial lasting 6 weeks comparing ruxolitinib to *Jak2*^{V617F} deletion (Supplementary Fig. S8A). We saw a greater improvement in hematologic parameters, spleen weights (mean vehicle 457 mg vs. ruxolitinib 235 mg vs. tamoxifen 125 mg, $P \leq 0.0027$), restoration of histopathologic morphology in both bone marrow and spleen, and reduced Cd45.2-mutant chimerism in peripheral blood (mean vehicle 40.7% vs. ruxolitinib 37.7% vs. tamoxifen 17.3%, $P \leq 0.0059$) of *Jak2*^{V617F}-deleted mice versus ruxolitinib-treated mice (Fig. 3E and F; Supplementary Fig. S8B–S8D). Reductions in total erythroid progenitors were observed with both ruxolitinib- and tamoxifen-treated mice by the conclusion of the study (mean vehicle 0.55×10^6/mL vs. ruxolitinib 0.28×10^6/mL vs. tamoxifen 0.21×10^6/mL, $P \leq 0.001$), with a greater effect on megakaryocytic progenitor (mean vehicle 0.55×10^6/mL vs. ruxolitinib 0.53×10^6/mL vs. tamoxifen 0.23×10^6/mL, $P \leq 0.05$) and total megakaryocyte output with *Jak2*^{VF} deletion specifically (Supplementary Fig. S8E–S8H). Most importantly, the reduction in mutant cell fraction seen with *Jak2*^{V617F} deletion within hematopoietic progenitor (GMP: $P \leq 0.0001$, MEP: $P \leq 0.0001$) and LSK stem cell–enriched populations was not observed with pharmacologic type I JAK inhibition (mean vehicle 87.9% vs. ruxolitinib 87.6% vs. tamoxifen 28.7%, $P \leq 0.0001$; Fig. 3G).

We previously showed that the type II JAK2 inhibitor CHZ868 showed improved efficacy compared with ruxolitinib *in vivo* (36). Consistent with these observations, treatment with CHZ868 showed greater efficacy than ruxolitinib with regard to improvement in hematologic parameters (mean Hct: CHZ868 50.3% vs. ruxolitinib 85.8%, $P \leq 0.0001$) and spleen volume reduction (mean CHZ868 76 mg vs. ruxolitinib 235 mg, $P < 0.0001$), at par with *Jak2*^{V617F} deletion (Fig. 3E and F; Supplementary Fig. S8B and S8C). Significant reductions in MEP, GMP, and LSK-mutant allele burden, as well as in more committed MEP populations, were also observed in CHZ868-treated mice compared with vehicle/ruxolitinib-treated mice (LSK: $P \leq 0.02$, GMP: $P \leq 0.013$, MEP: $P \leq 0.013$), but not to the extent seen with *Jak2*^{V617F} deletion (Fig. 3G; Supplementary Fig. S8F and S8G). These data confirm that more potent, selective target inhibition, including with type II JAK inhibitors, offers the potential for greater therapeutic efficacy when compared with current type I JAK inhibitors.

Previous studies have suggested that MAPK signaling plays an important role in MPN disease cell survival in the setting of type I JAK inhibitor therapy (13), and recent work has implicated the MAPK-dependent factor YBX1 as a critical mediator of *JAK2*^{V617F}-mutant cell persistence (14). We observed distinct effects on MAPK activity by RNA-seq with ruxolitinib treatment versus *Jak2*^{V617F} deletion in comparison with vehicle-treated mice. Negative regulators of KRAS signaling were downregulated with ruxolitinib (NES = −1.64, FDR ≤ 0.0005) and upregulated with *Jak2*^{V617F} deletion (NES = 1.35, FDR ≤ 0.039) in MEPs, suggesting enhanced MAPK signaling with ruxolitinib and MAPK attenuation with *Jak2*^{V617F} deletion (Fig. 3H). IHC of bone marrow sections confirmed increased phospho-ERK abundance in ruxolitinib-treated mice that was abrogated with *Jak2*^{V617F} deletion (Fig. 3I), and genotype-specific scATAC-seq revealed increased accessibility of MAPK-mediated AP-1 factors FOS/JUN (37) within HSPCs of ruxolitinib-treated MF patients in comparison with untreated MF HSPCs consistent with enhanced MAPK activity (Supplementary Fig. S8I). Furthermore, expression of *Ybx1* in sorted murine cKit$^+$ cells was increased with ruxolitinib therapy but potently suppressed with *Jak2*^{V617F} deletion (mean relative expression: vehicle 1.37 vs. ruxolitinib 2.52 vs. tamoxifen 0.42, $P \leq 0.0094$; Fig. 3J). These data suggest that potent, mutant-specific *Jak2*^{V617F} targeting can abrogate pathologic MAPK signaling and YBX1-mediated persistence of *Jak2*^{V617F}-mutant HSPCs.

JAK2^{V617F} Dependency with Cooperative TET2 Loss

Previous studies of mutational order in primary MPN cells have shown that cooperating mutations in epigenetic regulators, including TET2, can precede the acquisition of JAK2^{V617F}

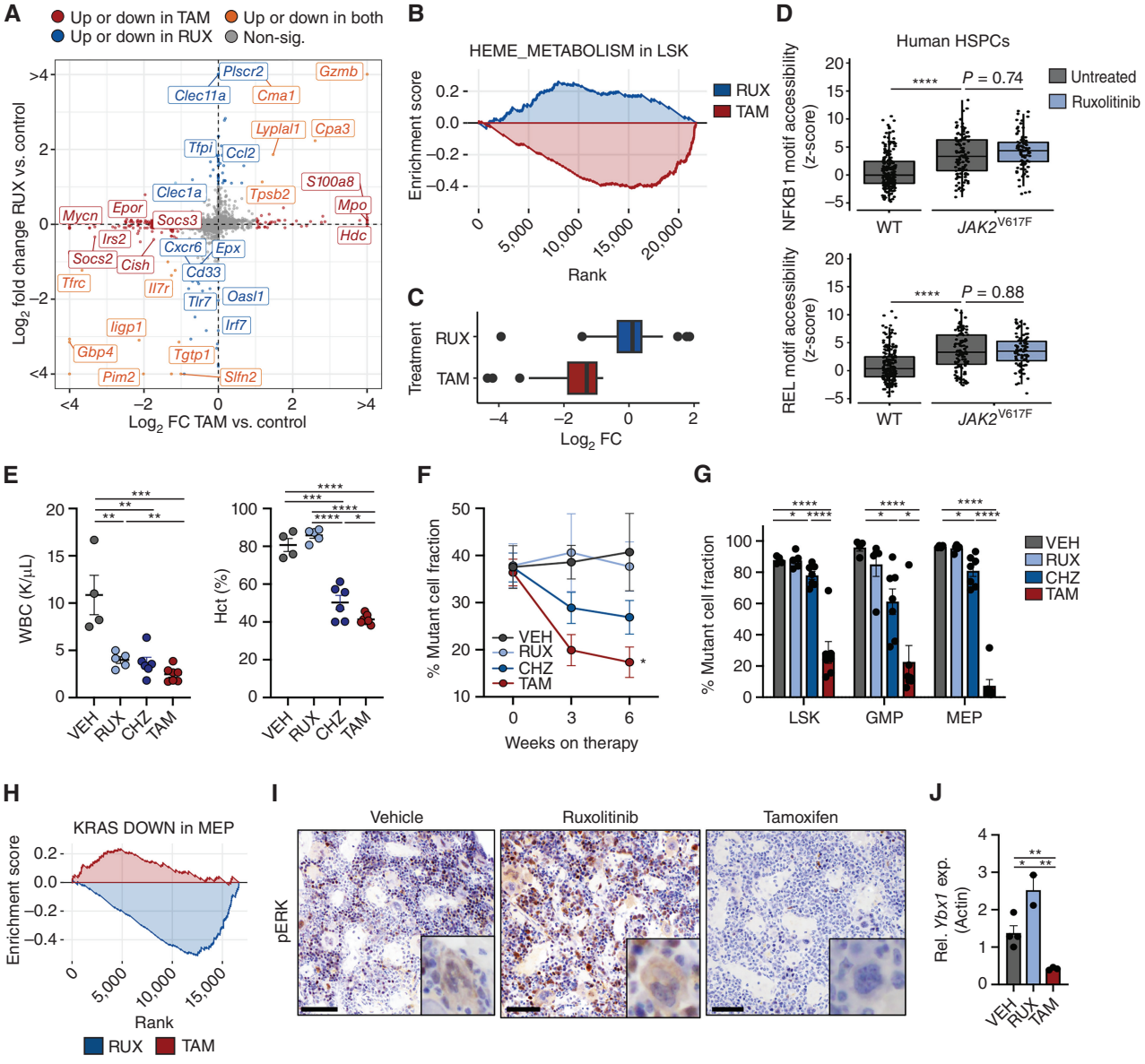

Figure 3. Differential efficacy of *Jak2*^{V617F} deletion compared with JAK inhibitor therapy. **A,** Scatter plot depicting $-\log_{10}(P_{adj})$*sign($\log_2$ Fold Change) of ruxolitinib (RUX) treated vs. tamoxifen (TAM; *Jak2*^{V617F}-deleted) treated LSKs (Lineage$^-$Sca1$^+$cKit$^+$) in comparison with MPN control LSKs isolated after 7 days of treatment ($n = 2$–3 biological replicates per arm); differentially expressed genes as indicated by color (see Supplementary Tables S1 and S3). **B,** Gene-set enrichment analysis (GSEA) depicting a positive enrichment in heme metabolism in ruxolitinib-treated ($n = 3$) vs. negative enrichment in tamoxifen (*Jak2*^{V617F}-deleted) treated ($n = 3$) LSKs isolated after 7 days of treatment. **C,** Box plot of the top leading edge genes in the Hallmark heme metabolism gene set of ruxolitinib-treated (blue) or tamoxifen (*Jak2*^{V617F}-deleted) treated (red) megakaryocytic-erythroid progenitor (MEP; Lineage$^-$cKit$^+$Sca1$^-$Cd34$^-$Fcg$^-$) cells as compared with untreated MPN cohorts. **D,** Box plots of scATAC-seq motif accessibility for either NFKB1 or REL transcription factors for untreated human *JAK2* WT ($n = 188$ cells from 4 patients; gray), untreated *JAK2*^{V617F}-mutant ($n = 105$ cells from 4 patients; gray), and ruxolitinib-treated *JAK2*^{V617F}-mutant ($n = 87$ cells from 3 patients; blue) HSPCs (35). *P* values indicated are from linear mixture model explicitly modeling patient identity as random effect to account for patient-specific effects, followed by likelihood ratio test. ****, $P \le 0.0001$. **E,** Peripheral blood counts of vehicle (VEH), ruxolitinib (RUX), the type II JAK2 inhibitor CHZ868 (CHZ), or tamoxifen (*Jak2*^{V617F}-deleted) treated mice at the conclusion of a 6-week *in vivo* trial: WBCs (left), Hct (right; $n \ge 4$ each; mean ± SEM). **, $P \le 0.01$; ***, $P \le 0.001$; ****, $p \le 0.0001$. **F,** Peripheral blood (PB) mutant Cd45.2 percent chimerism trend (0–6 weeks) of vehicle, ruxolitinib, CHZ868, or tamoxifen (*Jak2*^{V617F}-deleted) treated mice ($n \ge 4$ each; mean ± SEM). *, $P \le 0.05$. **G,** Bone marrow–mutant cell fraction of LSK (Lineage$^-$Sca1$^+$cKit$^+$), granulocytic-monocytic progenitor (GMP; Lineage$^-$cKit$^+$Sca1$^-$Cd34$^+$Fcg$^+$), and megakaryocytic-erythroid progenitor (MEP; Lineage$^-$cKit$^+$Sca1$^-$Cd34$^-$Fcg$^-$) compartments of vehicle, ruxolitinib, CHZ868, or tamoxifen (*Jak2*^{V617F}-deleted) treated mice at the conclusion of the 6-week *in vivo* trial ($n \ge 4$ each; mean ± SEM). *, $P \le 0.05$; ****, $P \le 0.0001$. **H,** GSEA depicting a negative enrichment in downregulation of KRAS signaling targets in ruxolitinib-treated ($n = 3$) vs. positive enrichment in tamoxifen (*Jak2*^{V617F}-deleted) treated ($n = 3$) MEPs isolated after 7 days of respective treatment. **I,** IHC of phospho-ERK on sectioned bone marrow of vehicle, ruxolitinib, or tamoxifen (*Jak2*^{V617F}-deleted) treated mice following 7 days of treatment ($n = 3$ individual biological replicates per arm). All images represented at 400× magnification. Scale bar, 20 μm. **J,** Quantitative PCR demonstrating relative *Ybx1* expression levels from isolated cKit$^+$ bone marrow of vehicle vs. ruxolitinib vs. tamoxifen (*Jak2*^{V617F}-deleted) treated mice after 7 days of treatment ($n = 2$–4 individual biological replicates per arm; mean ± SEM). *, $P \le 0.05$; **, $P \le 0.01$. **E–G,** Representative of $n = 3$ independent experiments.

in the clonal evolution of MPN and that antecedent *TET2* mutations can alter the *in vitro* sensitivity to ruxolitinib (38). In addition, *TET2* loss is the most frequently cooccurring mutation with *JAK2*^{V617F} in MPNs, and *in vitro* and *in vivo* studies have shown that concurrent *TET2* and *JAK2*^{V617F} mutations promote enhanced mutant HSC fitness and increased risk of MPN disease progression (39–41). Our *Jak2*^{RL} system allows for the assessment of JAK2^{V617F} dependency in the setting of cooccurring mutant allele activation/inactivation, including in the context of antecedent mutations in epigenetic regulators. We therefore assessed the impact of *Jak2*^{V617F} activation in concert with preexisting *Tet2* loss with the reversible *Jak2*^{RL} allele (Fig. 4A). Mice transplanted with *Dre*-electroporated *Ubc:CreER-Jak2*^{RL}*/Tet2*$^{-/-}$ cells demonstrated enhanced leukocytosis (mean 13.1 K/μL vs. 26.0 K/μL, $P \leq 0.001$) and thrombocytosis, increased spleen volumes (mean 317.6 mg vs. 612.2 mg, $P \leq 0.021$), and expanded mutant peripheral blood chimerism (mean 25.9% vs. 39.9%, $P \leq 0.025$) compared with *Ubc:CreER-Jak2*^{RL} and single-mutant *Tet2*$^{-/-}$-transplanted mice (Fig. 4B–D; Supplementary Fig. S9A). *Tet2*$^{-/-}$ and *Jak2*^{RL}*/Tet2*$^{-/-}$ HSCs also exhibited improved serial replating capacity in colony-forming assays compared to single-mutant *Jak2*^{RL} cells (Supplementary Fig. S9B). *Ex vivo* coculture of *Tet2*$^{-/-}$ and *Jak2*^{RL}*/Tet2*$^{-/-}$ cells over BMECs exhibited a near threefold increase in hematopoietic cell output (mean 2.92×10^6/mL vs. 2.41×10^6/mL vs. 0.80×10^6/mL, $P \leq 0.005$), including among Mac1$^+$ mature myeloid cells (mean 1.04×10^6/mL vs. 0.60×10^6/mL vs. 0.22×10^6/mL, $P \leq 0.023$), compared with *Jak2*^{RL} cells consistent with the known role of TET2 loss of function in enhancing myeloid lineage commitment (Supplementary Fig. S9C; ref. 42). Together, these data are phenotypically consistent with previous *Tet2*$^{-/-}$ and *Jak2*^{VF}*/Tet2*$^{-/-}$ models (39, 40) and highlight the utility of the Dre-Cre dual-recombinase system to model sequential acquisition of mutations *in vivo* and mimic the evolution of disease from a premalignant, clonally restricted hematopoietic state (i.e., single-mutant *Tet2*$^{-/-}$ knock-out) to overt MPN.

We next evaluated effects of *Jak2*^{V617F} deletion on *Jak2*^{RL}*/Tet2*$^{-/-}$–mutant cell fitness *in vivo* in competition with Cd45.1 bone marrow. Treatment with tamoxifen at 9 weeks posttransplant resulted in normalization of hematologic parameters ($P \leq 0.005$) and reductions in peripheral blood mutant cell fraction of double-mutant cells to a similar extent observed with *Jak2*^{V617F} deletion in single-mutant *Jak2*^{RL}-transplanted mice (Fig. 4E and F). Furthermore, spleen sizes (mean 103 mg vs. 529 mg, $P \leq 0.0001$) and total BM cellularity (femur; mean 11.6×10^6/mL vs. 15.7×10^6/mL, $P \leq 0.0035$) were similarly normalized with *Jak2*^{V617F} deletion (Supplementary Fig. S9D and S9E). Although the extent of reticulin fibrosis was increased in *Jak2*^{RL}*/Tet2*$^{-/-}$ mice compared with *Jak2*^{RL}, mutant allele reversal resolved fibrosis in both mutational contexts (Fig. 4G). The reduction in mutant cell fraction, as was observed with single-mutant mice, persisted down to the level of HSPCs in tamoxifen-treated *Jak2*^{RL}*/Tet2*$^{-/-}$ mice, including within the LSK stem cell–enriched compartment (mean tamoxifen 28.7% vs. MPN 73.7%, $P \leq 0.001$; Fig. 4H; Supplementary Fig. S9F). This decrease in mutant cell fraction appeared, at least in part, to be due to increased apoptosis, as *ex vivo* treatment with 4-OHT resulted in an increase in Annexin V$^+$ cells in *Jak2*^{RL} and double-mutant cells but not Tet2$^{-/-}$ cells (Supplementary Fig. S9G). This effect was specific to *Jak2*^{V617F} deletion, as treatment of *Tet2*$^{-/-}$ and *Jak2*^{RL}*/Tet2*$^{-/-}$ mice with type I JAK inhibition (ruxolitinib) did not alter allelic fraction (Supplementary Fig. S9H). Finally, in a subset of assayed *Jak2*^{RL}*/Tet2*$^{-/-}$ mice following *Jak2*^{V617F} deletion (4/9), we were unable to detect *Tet2*$^{-/-}$ knock-out bands in whole marrow at time of sacrifice. Cells harvested from *Jak2*^{RL}*/Tet2*$^{-/-}$ recipient mice following oncogenic deletion were unable to serially replate, indicating loss of self-renewal capacity in comparison with control double-mutant mice (Fig. 4I; Supplementary Fig. S9I). These data support the notion that cooccurring loss-of-function mutations of TET2 do not dramatically alter reliance on JAK/STAT signaling for disease maintenance and that, despite the fitness advantage engendered by TET2 loss on MPN HSCs, the reductions in HSC fitness in the setting of *Jak2*^{V617F} reversion suggest a unique dependency on oncogenic JAK2^{V617F} that renders double-mutant cells susceptible to eradication.

DISCUSSION

Mutated kinases occur frequently in cancer and are amenable to targeted inhibition; however, mechanisms mediating acquired resistance have been observed for most targeted therapies (43). In contrast, current JAK inhibitors fail to eliminate *JAK2*^{V617F}-mutant clones in patients with MPN, suggesting inadequate target inhibition and/or other genetic/nongenetic factors mediate *JAK2*^{V617F}-mutant cell persistence in the setting of JAK inhibitor therapy (44). We show in preclinical models that there is an absolute requirement for JAK2^{V617F} in MPN cells and that mutant-specific targeting of JAK2^{V617F} abrogates MPN features, reduces mutant cell fraction, and extends overall survival with concomitant depletion of disease-sustaining stem cells within the HSPC compartment. Furthermore, our data suggest that JAK2^{V617F} dependency persists even in the setting of antecedent mutations in epigenetic regulators, specifically *TET2*. Moreover, we demonstrate the feasibility of our dual-recombinase system to evaluate oncogenic signaling dependencies *in vivo*, and we believe that a similar approach will allow us to assess oncogenic dependencies and mechanisms of mutant-mediated transformation across a spectrum of malignant contexts.

These data support the notion that improved targeting of aberrant JAK2 signaling and downstream effectors offers greater therapeutic potential than current JAK kinase inhibitors and that JAK2^{V617F} mutant–selective inhibition represents a potential curative strategy for the treatment of patients with MPN. Clinical translation may include more potent JAK kinase inhibitors that inhibit both mutant and WT JAK2, as shown preclinically with the type II JAK inhibitor CHZ868 in MPN models and in B-cell acute lymphoid leukemia (ALL; refs. 36, 45). Recent data highlight the potential for selective targeting of mutant calreticulin (CALR) in MPNs (46), and the elucidation of the first full-length mutant JAK kinase structure (47) provides a path to the development of true mutant-specific JAK2^{V617F} inhibitors. As more potent (type II JAK2 inhibitors) and mutant-selective JAK2^{V617F} inhibitors enter the clinic, we expect that these agents will show increased efficacy, including the ability to substantively reduce mutant allele burden. Our studies suggest that therapeutic agents that

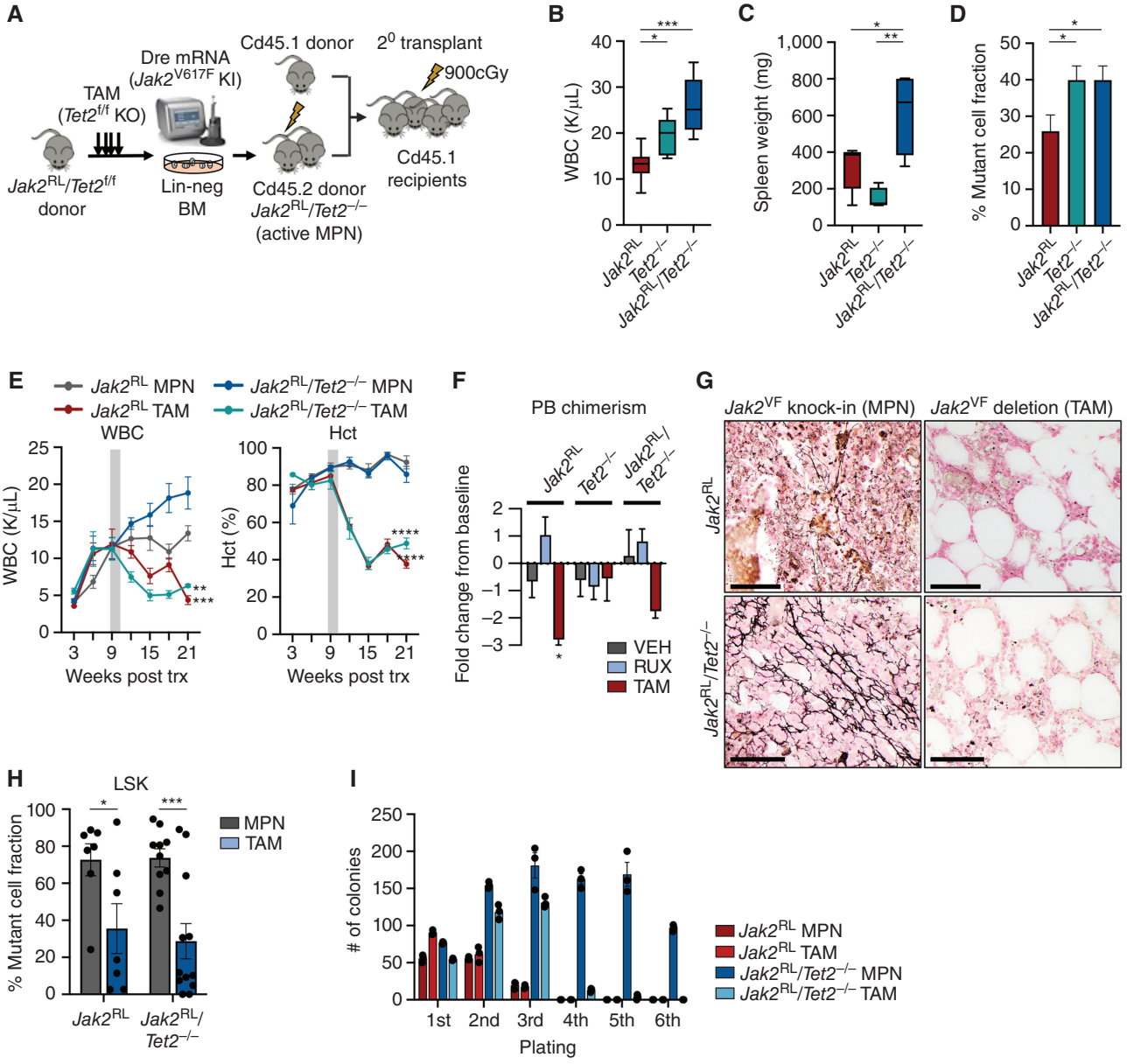

Figure 4. Jak2^{V617F} dependency with cooperative Tet2 loss. **A,** Schematic of the experimental setup for the double-mutant *Jak2*^{RL}/*Tet2*$^{f/f}$ competitive transplants. Downward arrows represent initial pulse tamoxifen (TAM) administration to genetically inactivate *Tet2*. **B,** WBC counts of primary *Jak2*^{RL} vs. *Tet2*$^{-/-}$ vs. *Jak2*^{RL}/*Tet2*$^{-/-}$ transplanted mice at 16 weeks posttransplant ($n = 5$–6 each; mean ± SEM). Representative of $n = 2$ independent transplants. *, $P \le 0.05$; ***, $P \le 0.001$. **C,** Spleen weights of primary *Jak2*^{RL} vs. *Tet2*$^{-/-}$ vs. *Jak2*^{RL}/*Tet2*$^{-/-}$ transplanted mice at time of sacrifice ($n = 5$–6 each; mean ± SEM). Representative of $n = 2$ independent transplants. *, $P \le 0.05$; **, $P \le 0.01$. **D,** Peripheral blood Cd45.2-mutant percent chimerism of *Jak2*^{RL} vs. *Tet2*$^{-/-}$ vs. *Jak2*^{RL}/*Tet2*$^{-/-}$ secondary competitive transplant mice at 9 weeks posttransplant ($n \ge 10$ per arm; mean ± SEM). Representative of $n = 2$ independent transplants. *, $P \le 0.05$. **E,** Peripheral blood count trends (weeks 0–21) of MPN vs. tamoxifen (*Jak2*^{V617F}-deleted) treated *Jak2*^{RL} vs. *Jak2*^{RL}/*Tet2*$^{-/-}$ competitive transplant mice: WBCs (left), hematocrit (Hct; right; $n = 3$–4 per arm; mean ± SEM). Gray bars represent duration of tamoxifen pulse/chow administration. Representative of $n = 2$ independent transplants. **, $P \le 0.01$; ***, $P \le 0.001$; ****, $P \le 0.0001$. **F,** Fold change from baseline (pretreatment) to posttreatment of Cd45.2-mutant peripheral blood chimerism of *Jak2*^{RL} vs. *Tet2*$^{-/-}$ vs. *Jak2*^{RL}/*Tet2*$^{-/-}$ transplanted mice treated for 6 weeks with either vehicle, ruxolitinib (RUX; 60 mg/kg twice daily), or tamoxifen (*Jak2*^{VF} deletion; $n = 4$–5 per arm; mean ± SEM). *, $P \le 0.05$. **G,** Reticulin stains of bone marrow from MPN vs. tamoxifen (*Jak2*^{V617F}-deleted) treated *Jak2*^{RL} vs. *Jak2*^{RL}/*Tet2*$^{-/-}$ mice at timed sacrifice (21 weeks). Representative micrographs of $n = 3$ individual mouse replicates per arm. All images represented at 400× magnification. Scale bar, 20 μm. **H,** Bone marrow–mutant Cd45.2 percent chimerism within the LSK (Lineage$^-$Sca1$^+$cKit$^+$) compartment of MPN vs. tamoxifen (*Jak2*^{V617F}-deleted) treated *Jak2*^{RL} vs. *Jak2*^{RL}/*Tet2*$^{-/-}$ mice at timed sacrifice (21 weeks; $n \ge 7$ biological replicates per arm across two independent transplants; mean ± SEM). *, $P \le 0.05$; ***, $P \le 0.001$. **I,** Serial replating assay of plated MPN vs. tamoxifen (*Jak2*^{V617F}-deleted) treated *Jak2*^{RL} vs. *Jak2*^{RL}/*Tet2*$^{-/-}$ bone marrow cells harvested at timed sacrifice 21 weeks and scored at day 8 after each plating (each sample plated in triplicate, representative of $n = 2$ independent experiments, mean ± SD). cGy, centigray; KI, knock-in; KO, knock-out; Lin-neg BM, lineage-negative bone marrow; trx, transplant.

more potently inhibit constitutive JAK2 signaling will offer greater benefit to patients with MPN than current therapies, including in the presence of cooperating clonal hematopoiesis disease alleles.

METHODS

Experimental Animals

All animal studies were performed in accordance with institutional guidelines established by Memorial Sloan Kettering Cancer Center (MSKCC) under the Institutional Animal Care and Use Committee–approved animal protocol (#07-10-016) and the Guide for the Care and Use of Laboratory Animals (National Academy of Sciences 1996). All experimental animals were maintained on a 12-hour light–dark cycle with access to water and standard chow *ad libitum*. Veterinary staff provided regular monitoring and husbandry care. All mice had intact immune systems, were drug and test naïve, and had not been involved in previous procedures. Animals were monitored daily for signs of disease or morbidity, bleeding, failure to thrive, infection, or fatigue and sacrificed immediately if they exhibited any of the above signs. Mice harboring the *Jak2*^{RL} allele were generated by Ingenious Targeting Laboratory in a C57BL/6J background. Specifically, a 8.86-kb genomic DNA used to construct the targeting vector was first subcloned from a positively identified C57BL/6J BAC clone (RP23-316C6). The region was designed such that the long homology arm (LA) extends ~6 kb 5′ to the cluster of Lox2272-Rox-Rox12-Lox2272 sites, and the short homology arm (SA) extends about 2.2 kb 3′ to the Neo cassette and 3′ Rox12 site. The inversion cassette is in between the second set of Lox2272 and Rox sites, and it consists of the mutant exon 14* (V617F) and its flanking genomic sequences for correct splicing (SaE14*Sd). The inversion cassette replaces WT exon 14 and the same flanking genomic sequences included in the cassette. The BAC was subcloned into a ~2.4 kb pSP72 (Promega) backbone vector containing an ampicillin selection cassette for retransformation of the construct. Ten micrograms of the targeting vector was then linearized and transfected by electroporation of FLP C57BL/6J (B6) embryonic stem cells. After selection with G418 antibiotic, surviving clones were expanded for PCR analysis to identify recombinant ES clones. After successful clone identification, the neomycin cassette was removed with a transient pulse of Cre recombinase and clones were reconfirmed following expansion. Finally, ES cells were injected in C57BL/6J mice via tetraploid complementation (NYU). *Tet2*$^{f/f}$ conditional knock-out mice, Cre-*lox Jak2*^{V617F} knock-in mice, RC::RLTG reporter mice, Cre TdTomato reporter mice, and *Ubc:CreER* mice have been described previously (2, 22, 25, 42, 48). Six- to 8-week-old female and male *Jak2*^{RL} or *Jak2*^{RL}/*Tet2*$^{f/f}$ donor mice were used for Dre electroporation knock-in experiments. Age-matched 6- to 10-week-old female mice were used as donors for all transplant experiments (Ly5.1 Cd45.1 competitive or C57BL/6J noncompetitive). All Jak2^{RL} donor mice used were crossed in a heterozygous fashion so as to retain a WT copy of JAK2.

Mouse Genotyping

DNA was isolated using the DNeasy Blood & Tissue Kit (Qiagen). The presence of the *Jak2*^{RL} locus was genotyped using the following primers: forward: 5′-CGTGCATAGTGTCTGTGGAAGTC-3′; reverse: 5′-CGTGGAGAGTCTGTAAGGCTCAA-3′. The WT allele gives a band of 246 bp; the mutant allele gives a band of 833 bp. *Jak2*^{V617F} knock-in genotyping was carried out with the following primers: forward: 5′-GCCATCTTTCCAGCCTAAAATTAG-3′; reverse: 5′-TCCAAAGAGTCTGTAAGTACAGAACT-3′ and with the following reaction conditions: 94°C for 3 minutes followed by 15 cycles of 94°C for 15 seconds, 65°C for 15 seconds, and 72°C for 30 seconds decreasing by 1°C per cycle, which is then followed by an additional 25 cycles of 94°C for 15 seconds, 50°C for 15 seconds, and 72°C for 30 seconds. *Jak2*^{V617F} knock-out genotyping was carried out using the following primers: forward: 5′-GCCATCTTTCCAGCCTAAAATTAG-3′; reverse: 5′-ACCAGTTGCTCCAGGGTTACACG-3′ and with the following reaction conditions: 94°C for 2 minutes followed by 30 cycles of 94°C for 30 seconds, 53°C for 30 seconds, and 72°C for 30 seconds. Sequencing of the unrecombined Rox-lox locus was carried out using the following primers: forward: 5′-AGGAGCATCGATGACTACATGATGAG-3′; reverse: 5′-AGACTCTCCACGGTCTCATCTACG-3′ and with the following reaction conditions: 98°C for 30 seconds followed by 35 cycles of 98°C for 10 seconds, 65°C for 15 seconds, and 72°C for 30 seconds. *Tet2* genotyping were carried out using the following primers/conditions: forward: 5′-AAGAATTGCTACAGGCCTGC-3′; reverse: 5′-TTCTTTAGCCCTTGCTGAGC-3′; ExR: 5′-TAGAGGGAGGGGGCATAAGT-3′ and with the following reaction conditions: 94°C for 2 minutes followed by 39 cycles of 94°C for 35 seconds, 58°C for 45 seconds, and 72°C for 55 seconds. Annotation of PCR genotyping results was carried out on a QIAxcel Advanced System (Qiagen) and analyzed using QIAxcel ScreenGel software (Qiagen). Sanger sequencing was performed by Genewiz and analyzed using Benchling software.

Dre mRNA Electroporation

Dre mRNA was purchased from TriLink Biotechnologies and electroporation carried out using the Neon Transfection System (Thermo Fisher Scientific) as per the manufacturer's protocol. Specifically, bone marrow donor cells were isolated from limb bones into PBS (pH 7.2) containing 2% FCS via centrifugation. After red blood cell (RBC) lysis, single-cell suspensions were depleted of lineage-committed hematopoietic cells using a Lineage Cell Depletion Kit according to manufacturer's protocol (EasySep, StemCell Technologies, Inc.). A total of 2.5–3.0 × 10^6 lineage-depleted bone marrow was then washed in PBS and then resuspended in 135 μL Buffer T, to which 15 μL of *Dre* mRNA (at 1 μg/μL) was quickly added and electroporated at the following conditions: 1,700V for 20 ms ×1 pulse. The cells were then pipetted into penicillin–streptomycin free StemSpan SFEM medium with thrombopoietin (TPO; 20 ng/mL; PeproTech) and stem cell factor (SCF; 20 ng/mL; PeproTech), cultured for 2 hours, and then subsequently harvested and washed/resuspended in PBS and transplanted via lateral tail vein injection into lethally irradiated (900 cGy) 6- to 8-week-old C57BL/6J recipient mice at approximately 4 × 10^5 cells per recipient along with 50,000 unelectroporated WT whole bone marrow support cells. Single-mutant *Tet2*$^{-/-}$ or double-mutant *Jak2*^{RL}/*Tet2*$^{-/-}$ transplants/electroporations were carried out as above, except donor mice were dosed with tamoxifen (100 mg/kg by oral gavage daily ×4; purchased from MedChemExpress) 6–8 weeks prior to harvest and excision confirmed prior to *Dre* electroporation.

Transplantation Assays and In Vivo Experiments

Jak2^{RL}, *Tet2*$^{f/f}$, and *Jak2*^{RL}/*Tet2*$^{f/f}$ lines were crossed to *Ubc:CreER* tamoxifen-inducible Cre lines and RLTG dual-recombinase reporter lines (25, 48). Primary recipient mice transplanted with *Dre* mRNA-recombined *Ubc:CreER-Jak2*^{RL}, *Ubc:CreER-Tet2*$^{-/-}$, or *Ubc:CreER-Jak2*^{RL}/*Tet2*$^{-/-}$ bone marrow cells were bled every 3–4 weeks posttransplant to monitor disease status. Peripheral blood was isolated by submandibular bleeds, and complete blood counts were determined using a ProCyte Dx (IDEXX Laboratories) per manufacturer's instruction. For competitive repopulation assays, 1.2 × 10^6 whole bone marrow from primary transplant recipient mice exhibiting MPN was harvested 6–8 weeks posttransplant and combined with age-matched 0.8 × 10^6 Cd45.1 (Jackson Laboratories) whole bone marrow and transplanted into 6- to 8-week-old lethally irradiated Cd45.1 secondary recipient mice. Mice transplanted with Dre-recombined *Jak2*^{V617F} cells demonstrating low Cd45.2 chimerism at baseline (<15%) and/or evidence of poor MPN cell engraftment were excluded from study cohorts. To induce Cre and delete *Jak2*^{V617F}, mice were treated with

tamoxifen (purchased from MedChemExpress) 100 mg/kg daily (dissolved in corn oil) by oral gavage × 4 followed by 14 days of tamoxifen chow (80 mg/kg daily; ENVIGO). Tamoxifen control studies were carried out using similar dosing schedules on 45.1 mice transplanted in competition with *Dre*-electroporated, Cre-negative *Jak2*^{RL} MPN bone marrow cells. For terminal tissue isolation, mice were euthanized with CO_2 asphyxiation, and tissues were dissected and fixed with 4% paraformaldehyde for histopathologic analysis. For whole bone marrow isolation, the femurs, hips, and tibias were dissected and cleaned. Cells were then isolated using centrifugation at 8,000 × *g* for 1 minute followed by RBC lysis (BioLegend) for 10–15 minutes. Bone marrow cell numbers and viability were determined using an automated cell counter (ViCell Blu, Beckman Coulter). Spleen cell suspensions were generated by crushing whole spleen and filtering through a 70-μm filter. RBC lysis (BioLegend) was performed, and cells were prepared for downstream processing or frozen.

In Vivo *Drug Studies*

For *in vivo* inhibitor studies, approximately 8 weeks after transplant, secondary transplant cohorts of lethally irradiated mice transplanted with *Ubc:CreER-Jak2*^{RL} bone marrow in competition with Cd45.1 marrow (as above) and exhibiting active MPN were bled and cohorted on the basis of peripheral blood Cd45.2 chimerism and total WBC count to achieve congruency across treatment arms. Mice were then treated with ruxolitinib (60 mg/kg orally twice daily; dissolved in 20% Captisol in PBS; purchased from MedChemExpress), CHZ868 (30 mg/kg orally daily; dissolved in 0.5% methylcellulose + 0.5% Tween-80 in dH_2O; purchased from MedChemExpress), tamoxifen to delete *Jak2*^{V617F} (as above; purchased from MedChemExpress), or vehicle. Investigators were not blinded to the identity of mice or samples. Mice were treated for a total of 6 weeks before timed sacrifice and marrow/spleen harvested as above.

BMEC Culture

Bone marrow cells were isolated from limb bones into FACS buffer (PBS + 2% FBS) via centrifugation. After RBC lysis, single-cell suspensions were depleted of lineage-committed hematopoietic cells using a Lineage Cell Depletion Kit according to manufacturer's protocol (EasySep, StemCell Technologies, Inc.). Subsequently, 50,000 of the resulting lineage$^-$ cells were plated on a confluent monolayer of BMECs in a single well of a 12-well plate. Each well had 1 mL StemSpan SFEM (StemCell Technologies, Inc.) with 20 ng/mL recombinant murine SCF (PeproTech) in addition to the corresponding drug treatment: either 4-OHT (Sigma Aldrich; stock concentration: 13 mmol/L) or its vehicle, appropriately diluted in media to its final concentration [i.e., 0.01% (v/v) of ethanol (EtOH), or 200 nmol/L, 400 nmol/L or 1 μmol/L of 4-OHT; three replicates/condition]. The BMECs were seeded 2 days before plating the lineage$^-$ cells at a density of 100,000 cells/well. Cocultures were maintained for a total of 7 days at 37°C and 5% CO_2, with media being completely refreshed with the original SCF and drug/vehicle concentrations. 4-OHT or EtOH vehicle was added to the culture on day 1 and again on day 4. On day 7, total cells were harvested with Accutase (BioLegend) and cell numbers were determined via an automatic cell counter (ViCell Blu, Beckman Coulter). Cells were then stained with the desired antibody cocktail and phenotyped by flow cytometry.

Flow Cytometry, Cell Sorting, and Western Blot Analysis

After single-cell preparation, murine peripheral blood, whole bone marrow, or spleen mononuclear cells were lysed for 10–15 minutes with RBC lysis buffer (BioLegend) and washed twice with FACS buffer. Cells were then resuspended in Fc (Cd16/32) block for 15 minutes and then subsequently stained with a cocktail comprised of antibodies targeting Cd3 (17A2), Cd45R/B220 (RA3-6B2), Gr-1 (RB6-8C5), Cd11b (M1/70), Cd45.2 (104), and Cd45.1 (A20) for 30 minutes. For hematopoietic stem/progenitor cell analysis, lysed bone marrow was stained with a cocktail of lineage markers along with antibodies against cKit (2B8), Sca1 (D7), FcγRII/III (2.4G2), Cd34 (RAM34), Cd150 (9D1), and Cd48 (HM48-1). Erythroid progenitor flow was carried out on unlysed bone marrow or spleen with the addition of the following antibodies: Cd105 (43A3), Cd71 (R17217), Cd41 (MWReg30), and Ter119 (Ter-119). All FACS antibodies were purchased from BD, BioLegend, or eBioscience. Following antibody incubation, cells were washed with FACS buffer and resuspended in a 4′,6-diamidino-2-phenylindole (DAPI)-containing FACS buffer solution for analysis and sorting. Samples were run on an LSRFortessa (Becton Dickinson) using FACSDiva software and analyzed with FlowJo v10.8.1 (Treestar). For sorting of Cd45.2$^+$ lin$^-$Sca1$^+$cKit$^+$ experiments, whole bone marrow samples were stained with antibodies for lineage cocktail, cKit, and Sca1 as well as Cd45.2 and Cd45.1 as above and gated and sorted on Lin$^-$cKit$^+$Sca1$^+$ Cd45.2$^+$ fractions using a FACSAria 3 (Becton Dickinson) instrument. Samples were subsequently spun at 1,500 rpm for 5 minutes, resuspended in Buffer ATL Cell Lysis solution (Qiagen), and DNA extracted using the DNA Micro Kit (Qiagen) as per the manufacturer's instructions. For Western blot analysis, whole-cell protein extracts from harvested splenocytes were prepared using RIPA buffer (Thermo Fisher Scientific) containing a protease/phosphatase inhibitor cocktail (Thermo Fisher Scientific). Protein quantification was performed using the Pierce BCA protein assay kit (Thermo Fisher Scientific) and analyzed on a Cytation 3 plate reader (BioTek). Proteins were separated by NuPAGE 4%–12% Bis-Tris Gel and transferred to a nitrocellulose membrane. The following antibodies were used: β-actin (Cell Signaling Technology, 4970S), STAT5 (Cell Signaling Technology, 94205S), and pSTAT5 (Cell Signaling Technology, 9359S). Images were obtained using the ChemiDoc Imaging System (Bio-Rad) and analyzed using ImageLab software (Bio-Rad).

Histology Staining, IHC, and Photography

Tibia and spleen samples were fixed in 4% paraformaldehyde for more than 24 hours and then embedded in paraffin. Paraffin sections were cut on a rotary microtome (Mikrom International AG), mounted on microscope slides (Thermo Fisher Scientific), and air-dried in an oven at 37°C overnight. After drying, tissue section slides were processed either automatically for hematoxylin and eosin (H&E) staining (COT20 stainer, Medite) or manually for reticulin staining. All samples and slide preparation, including IHC, were carried out at the Tri-Institutional Laboratory of Comparative Pathology (LCP) core facility. The following antibodies were used for IHC: Mac1 (Cedarlane CL8941B, 1:100), Ter119 (BD Biosciences, 550565 1:200), and p-44/42 MAPK (Erk1/2; Cell Signaling Technology, 4376, 1:100). Pictures were taken at 100×, 200×, and 400× (H&E, reticulin, and respective IHC) magnification using an Olympus microscope and analyzed with Olympus Cellsens software. Tissue sections were formally evaluated by a hematopathologist (W. Xiao), including reticulin scoring.

Assessment of Cell Cycle, Apoptosis, and Viability

Apoptosis was measured by flow cytometry on a LSRFortessa (Becton Dickinson) cytometer with Annexin V PerCPCy5.5 antibody (BioLegend) in combination with the antibody cocktail (above) in Annexin binding buffer (BioLegend) at 1:50 dilution in combination with DAPI as live/dead cell stain. For cell-cycle analysis, lineage-negative marrow was surface stained with the LSK antibody cocktail above followed by the Zombie UV Fixable Viability Kit (BioLegend) and then subsequently fixed and permeabilized using the FIX&PERM Cell Permeabilization Kit (Invitrogen) as per the manufacturer's instructions and stored at −20°C until further staining. Cells were then washed twice in FACS buffer, pelleted, and stained with anti–Ki-67 antibody (BioLegend) or isotype control for 30 minutes; washed again; and

resuspended in FACS buffer with DAPI. Samples were run on linear for DAPI stain.

Colony-Forming Assays

To assess colony formation and serial replating capacity, 50,000 RBC-lysed whole bone marrow cells were seeded in 1.5 mL MethoCult M3434 (StemCell Technologies) with no additional supplemental cytokines in triplicate on 6-well plates and scored on day 8. For replating, cells were harvested and pooled and then reseeded once more at 50,000 cells/well in 1.5 mL MethoCult M3434 in triplicate. We assessed *Dre* mRNA-mediated recombination efficiency both pretransplant and posttransplant using either freshly *Dre*-electroporated *Jak2*^{RL} lineage-negative bone marrow cells or whole marrow harvested 6 weeks following transplant from primary recipient mice transplanted with *Dre*-electroporated *Jak2*^{VF} knock-in marrow. These cells were seeded as above, and after 7 days, individual colonies were plucked into 70 μL of Buffer ATL and DNA extraction was carried out using the DNA Micro Kit (Qiagen) as per the manufacturer's instructions.

Serum Cytokine Profiling

Serum samples were diluted two-fold with PBS (pH 7.2) and stored at −80°C until analysis. Cytokine assays were carried out using the Millipore Mouse Cytokine 32-plex kit and FlexMAP 3D platform (Luminex) per the manufacturer's instructions. xPONENT (Luminex) and Milliplex Analyst Software (Millipore) were used to convert mean fluorescent intensities (MFI) values into molecular concentrations using a standard curve (5-parameter logistic fitting method). Data were then normalized by first transforming concentration values using the $\log_2$ function and the mean and SD of the log values calculated across all samples for each analyte. Z-scores were then computed using the formula Z-score = (mean of $\log_2$ concentration values for an analyte per condition − mean of average $\log_2$ values for an analyte across all conditions)/SD calculated across the three conditions (WT, MPN, tamoxifen) and then used to normalize the cytokine data. The heat map was generated using the R package tidy_heatmap to visualize Z-score normalization for cytokines that displayed differential expression across the groups.

RNA-seq and Data Analysis

For gene expression analysis, secondary cohorts of lethally irradiated C57BL/6J mice transplanted with *Ubc:CreER-Jak2*^{RL}-RLTG reporter bone marrow 8 weeks posttransplant and exhibiting MPN were treated with ruxolitinib (60 mg/kg orally twice daily), and tamoxifen (100 mg/kg by oral gavage daily × 4 followed by 80 mg/kg of tamoxifen chow × 3 days) ± vehicle (MPN control) for 7 days and then sacrificed. Lineage-depleted bone marrow was isolated and stained with an antibody cocktail containing a combination of lineage markers along with antibodies against cKit (2B8), Sca1 (D7), FcγRII/III (2.4G2), and Cd34 (RAM34) for 30 minutes; washed; and then resuspended in FACS buffer containing DAPI as a live/dead stain. TdTomato$^+$ (*Jak2*^{RL} knock-in) or GFP$^+$ (*Jak2*^{RL} knock-out) LSKs and MEPs were then sorted on a FACSAria III directly into TRIzol LS (Invitrogen) and stored at −80°C until processing. RNA was subsequently isolated using the Direct-Zol Microprep Kit (Zymo Research, R2061) according to manufacturer's protocol and quantified using the Agilent High Sensitivity RNA ScreenTape (Agilent 5067–5579) on an Agilent 2200 TapeStation. cDNA was generated from 1 ng of input RNA using the SMART-Seq HT Kit (Takara 634455) at half reaction volume followed by Nextera XT (Illumina FC-131-1024) library preparation. cDNA and tagmented libraries were quantified using High Sensitivity D5000 ScreenTape (5067–5592) and High Sensitivity D1000 ScreenTape, respectively (5067–5584). Libraries were sequenced on a NovaSeq at the Integrated Genomics Operation (IGO) at MSKCC. FASTQ files were mapped and transcript counts were enumerated using STAR (genome version mm10 and transcript version M13). Counts were input into R and RNA-seq analysis using DESeq2. Genes were filtered out prior to modeling in DESeq if they were not detected in all, with MEPs and LSKs modeled separately. Differentially expressed genes were identified with a $\log_2$-fold change of 1 and an adjusted *P* value of 0.05. Gene-set enrichment analysis was performed using the fgsea package at 100,000 permutations with gene sets extracted from the msigdbr package. ssGSEA was performed using the gsva package. To determine the frequency of the *Jak2*^{V617F} allele and relative mutant expression, the samtools(v1.5)/mpileup variant calling tool was used. A minimum mapping quality of 30 for each read and default minimum base quality of 13 was used. Maximum depth was set to 100,000. Bcftools (v1.8) was used to convert BCF files into VCF files, and the vcfR (v1.14) package in R was used to parse the VCF files of alternative and reference alleles and read depth counts. Statistical differences between the different conditions were calculated using the one-sided Wilcoxon rank sum test. Figures were prepared using the ggplot2, ggsignif, ggrepel, and tidyheatmaps packages in R. Complete scripts can be found on github at https://github.com/bowmanr/goldilox.

Mouse ATAC-seq and Data Analysis

Chromatin accessibility assays utilizing the bacterial Tn5 transposase were performed as described previously (49). Briefly, 5.0×10^4 TdTomato$^+$ (*Jak2*^{RL} knock-in) or GFP$^+$ (*Jak2*^{RL} knock-out) cKit$^+$ bone marrow cells from mice treated for 7 days with tamoxifen or an untreated MPN control cohort were sorted on a FACSAria III directly into PBS and subsequently lysed and incubated with transposition reaction mix containing PBS, Tagment DNA buffer, 1% Digitonin, 10% Tween-20, and Transposase (lllumina). Samples were then incubated for 30 minutes at 37°C in a thermomixer at 1,000 rpm. Prior to amplification, samples were concentrated with the DNA Clean and Concentrator Kit-5 (Zymo). Samples were eluted in 20 μL of elution buffer and PCR-amplified using the NEBNext 2X Master Mix (NEB) for 11 cycles and sequenced on a NextSeq 500 (Illumina). All samples were processed at the Center for Epigenetics Research (CER) core facility at MSKCC. Libraries were sequenced on a NovaSeq at the Integrated Genomics Operation (IGO) at MSKCC. Data analysis was completed through in-house scripts at the CER, in brief: Reads were trimmed with "trim_galore" and aligned to mouse genome mm9 using bowtie2 (default parameters). Duplicates were removed with the Picard tool "MarkDuplicates," and peaks were called with MACS2, merged, and used to create a full peak atlas. Read counts were tabulated over this atlas using featureCounts. Downstream differential enrichment testing was completed in DESeq2 with default normalization scheme. HOMER was used for known motif enrichment amongst the differentially enriched peaks as defined by a fold change of ± 1.5 and an adjusted *P* value of 0.1. For the lineage deconvolution analysis presented in Supplementary Fig. S6H, we performed a process that uses a reference library from aggregated biological replicates across multiple cell types and selects key lineage-specific loci to deconvolve samples and generate component estimates (31). A nonnegative least-squares regression (NNLS) comparing each unknown sample to the set of normal hematopoietic states is then performed. Deconvolution coefficients are interpreted as proportions to estimate the magnitude per hematopoietic stage.

Human scATAC-seq and Data Analysis

scATAC-seq data were processed using cellranger-ATAC (v2.0.0) mkfastq. ATAC-sequencing reads were then aligned to the hg38 reference genome using cellranger-ATAC count function. Fragment files generated by cellranger-ATAC were used as input for the ArchR (ref. 50; v1.0.0). For initial dimensionality reduction and patient data integration, the cell by genomic bin matrix was used as input for reciprocal latent semantic indexing (LSI) as calculated by the Signac (v1.1.1). Transcription factor motif accessibility z-scores were

calculated with ChromVAR (ref. 51; v1.8.0). The earliest HSPCs (cluster HSPC1, ref. 35) were subset for downstream analysis, and statistical comparisons of motif accessibility for NFKB1, REL, FOS, and JUN transcription factors were performed via linear mixture model including patient identity as random effect to account for potential technical confounders arising from sample-specific batch effects. For heat map representation, motif accessibility z-scores were used as input and the pheatmap (v1.0.12) R package was used.

Quantitative Real-Time PCR

Total RNA was extracted from magnetic-bead isolated cKit$^+$ bone marrow (Miltenyi Biotec) using the Direct-zol RNA extraction kit (Zymo) as per the manufacturers' protocols, respectively. Complementary DNA was then reverse transcribed using the Verso cDNA Synthesis kit (Thermo Fisher Scientific). *Ybx1* expression was evaluated by quantitative reverse-transcription (qRT) PCR using TaqMan probes purchased from Thermo Fisher Scientific (Mm00850878_g1) on the RealPlex thermocycler (Thermo Fisher Scientific).

Statistical Analysis

Statistical analyses were performed using Student *t* test (normal distribution) using GraphPad Prism version 6.0h (GraphPad Software) unless otherwise noted. Kaplan–Meier curves were determined using the log-rank test. $P < 0.05$ was considered statistically significant. For the cytokine analysis presented in Fig. 1F and Supplementary Fig. S3J, individual cytokines were analyzed using the Kruskal–Wallis test with lower values set at the lower limit of the assay and *P* values generated by doing multiple comparisons testing across treatment arms (WT vs. MPN vs. tamoxifen) and adjusting based on FDR of ≤ 0.05. The number of animals, cells, and experimental replication can be found in the respective figure legends.

Data Availability

Raw and processed sequencing data are made available at https://github.com/bowmanr/goldilox and via the NCBI Gene-Expression Omnibus (GEO) at GSE203464.

Authors' Disclosures

A.J. Dunbar reports personal fees from Incyte outside the submitted work; in addition, A.J. Dunbar has a patent for PCT/US2023/066910 pending. R.L. Bowman reports a patent for PCT/US2023/066910 pending. F. Izzo reports grants from American Society of Hematology Fellow-to-Faculty Scholar Award during the conduct of the study. W. Xiao reports grants from Stemline therapeutics outside the submitted work. S.F. Cai reports a consultancy for and previously held equity interest in Imago Biosciences, neither of which is directly related to the content of this article. J.L. Glass reports grants from NIH during the conduct of the study and personal fees from GLG outside the submitted work. A.D. Viny reports other support from Arima Genomics outside the submitted work. R.P. Koche reports personal fees from Econic Biosciences outside the submitted work. S.C. Meyer reports grants from Swiss National Science Foundation, Cancer League Basel, Foundation "Stiftung für krebskranke Kinder Regio Basiliensis," and grants from Foundation for the Fight against Cancer during the conduct of the study; personal fees from Novartis, Celgene/BMS, GSK, OrphaSwiss GmbH, Ajax Therapeutics Inc.; other support from AbbVie AG; and other support from Amgen outside the submitted work. In addition, S.C. Meyer has a patent for PAT058952-US-PSP pending and a patent for PAT058953-US-PSP pending. D.A.L. is on the Scientific Advisory Board of Mission Bio, Alethiomics, Pangea, Quotient Therapeutics and C2i Genomics and has received prior research funding from BMS, 10X Genomics, Mission Bio, Ultima Genomics, Oxford Nanopore, and Illumina unrelated to the current manuscript. R.L. Levine reports other support from Ajax during the conduct of the study; in addition, R.L. Levine has a patent for JAK2V617F reversible mouse pending; is on the supervisory board of Qiagen; and is a scientific advisor to Imago, Mission Bio, Zentalis, Ajax, Auron, Prelude, C4 Therapeutics, and Isoplexis. R.L. Levine also receives research support from Ajax, Zentalis, and Abbvie; has consulted for Incyte, Janssen, and Astra Zeneca; and has received honoraria from Astra Zeneca for invited lectures. No disclosures were reported by the other authors.

Authors' Contributions

A.J. Dunbar: Conceptualization, data curation, formal analysis, funding acquisition, investigation, visualization, writing–original draft, writing–review and editing. **R.L. Bowman:** Conceptualization, resources, data curation, formal analysis, supervision, validation, investigation, visualization, writing–original draft. **Y.C. Park:** Investigation. **K. O'Connor:** Validation, investigation, methodology. **F. Izzo:** Conceptualization, formal analysis, validation, visualization, methodology. **R.M. Myers:** Conceptualization, formal analysis, validation, investigation, visualization, methodology, writing–original draft. **A. Karzai:** Investigation. **Z. Zaroogian:** Investigation. **W. Kim:** Validation, investigation. **I. Fernandez-Maestre:** Validation, investigation, visualization, methodology. **M.R. Waarts:** Investigation, visualization. **A. Nazir:** Investigation. **W. Xiao:** Validation, investigation, visualization, writing–original draft. **T. Codilupi:** Validation, investigation, visualization. **M. Brodsky:** Investigation. **M. Farina:** Investigation. **L. Cai:** Investigation. **S.F. Cai:** Investigation, visualization. **B. Wang:** Investigation. **W. An:** Investigation. **J.L. Yang:** Investigation, visualization, methodology. **S. Mowla:** Investigation. **S.E. Eisman:** Investigation. **A. Hanasoge Somasundara:** Investigation. **J.L. Glass:** Investigation. **T. Mishra:** Investigation. **R. Houston:** Investigation. **E. Guzzardi:** Investigation. **A.R. Martinez Benitez:** Investigation. **A.D. Viny:** Conceptualization, investigation. **R.P. Koche:** Conceptualization, data curation, formal analysis, investigation, methodology. **S.C. Meyer:** Investigation, visualization, methodology. **D.A. Landau:** Conceptualization, resources, data curation, formal analysis, funding acquisition, validation, investigation, visualization, methodology. **R.L. Levine:** Conceptualization, resources, data curation, formal analysis, funding acquisition, writing–original draft, project administration, writing–review and editing.

Acknowledgments

We are grateful to members of the Levine Lab for their discussion of the work. We would also like to acknowledge Dr. Alex Joyner (MSKCC), Dr. Patricia Jensen (NIH), and Dr. Tudor Badea (NIH) for discussion on Dre-Rox technology as well as Sime Brkic (University Hospital Basel Switzerland) for their technical advice and support. This work was supported by the NCI award P01 CA108671 (to R.L. Levine). R.L. Levine was supported by a Leukemia and Lymphoma Society Scholar award. A.J. Dunbar is a William Raveis Charitable Fund Physician-Scientist of the Damon Runyon Cancer Research Foundation (PST-24-19). He also has received funding from the NIH (T32CA009207), AACR (17-40-11-DUNB), and the American Association of Clinical Oncology. R.L. Bowman was supported by a Damon Runyon-Sohn Fellowship and the NCI (K99CA248460). R.M. Myers is supported by a Medical Scientist Training Program grant from the National Institute of General Medical Sciences of the NIH under award number T32GM007739 to the Weill Cornell/Rockefeller/Sloan Kettering Tri-Institutional MD-PhD Program and by the Weill Cornell Medicine NYSTEM Training Program under award number C32558GG. F. Izzo is supported by the American Society of Hematology Fellow-to-Faculty Scholar Award. W. Xiao is supported by Alex's Lemonade Stand Foundation and the Runx1 Research Program, a Cycle for Survival's Equinox Innovation Award in Rare Cancers, MSK Leukemia SPORE (Career Enhancement Program, NIH/NCI P50 CA254838-01), and an NCI grant (K08CA267058-01). S.F. Cai is supported by a Career Development Award from the NCI (K08CA241371-01A1).

J.L. Glass is supported by a K08 through the NIH (CA230172). A.D. Viny is supported by the National Cancer Institute MERIT award (R37CA286857), an EvansMDS Discovery grant from the Edward P. Evans Foundation, a Clinical Investigator grant from the Damon Runyon Cancer Research Foundation (120-22), a Clinician Scientist Development grant from the Doris Duke Charitable Foundation, and grants from the Columbia University Vagelos College of Physicians & Surgeons (Gerstner Scholar and Early Career Physician Scientist). S.C. Meyer receives funding from the Swiss National Science Foundation (PZ00P3_161145, PCEFP3_181357), the Cancer League Basel and the "Stiftung für krebskranke Kinder Regio Basiliensis" (KLbB-4784-02-2019), and the Foundation for the Fight against Cancer. D.A. Landau is supported by the Burroughs Wellcome Fund Career Award for Medical Scientists, Valle Scholar Award, Leukemia Lymphoma Scholar Award, the MacMillan Family Foundation and the MacMillan Center for the Study of the Non-Coding Cancer Genome at the New York Genome Center, and the Mark Foundation Emerging Leader Award as well as the Tri-Institutional Stem Cell Initiative, the National Heart Lung and Blood Institute (R01HL145283; R01HL157387-01A1), the NCI (R33 CA267219), the National Human Genome Research Institute, Center of Excellence in Genomic Science (RM1HG011014), and the NIH Common Fund Somatic Mosaicism Across Human Tissues (UG3NS132139). Studies supported by MSK core facilities were supported in part by MSKCC Support Grant/Core Grant P30 CA008748 and the Marie-Josée and Henry R. Kravis Center for Molecular Oncology. R.L. Levine is also supported by a Leukemia & Lymphoma Society Specialized Center of Research grant.

Note

Supplementary data for this article are available at Cancer Discovery Online (http://cancerdiscovery.aacrjournals.org/).

Received August 26, 2022; revised November 29, 2023; accepted January 10, 2024; published first January 12, 2024.

REFERENCES

1. Levine RL, Pardanani A, Tefferi A, Gilliland DG. Role of JAK2 in the pathogenesis and therapy of myeloproliferative disorders. Nat Rev Cancer 2007;7:673–83.
2. Mullally A, Lane SW, Ball B, Megerdichian C, Okabe R, Al-Shahrour F, et al. Physiological Jak2V617F expression causes a lethal myeloproliferative neoplasm with differential effects on hematopoietic stem and progenitor cells. Cancer Cell 2010;17:584–96.
3. Mullally A, Poveromo L, Schneider RK, Al-Shahrour F, Lane SW, Ebert BL. Distinct roles for long-term hematopoietic stem cells and erythroid precursor cells in a murine model of Jak2V617F-mediated polycythemia vera. Blood 2012;120:166–72.
4. Bhagwat N, Koppikar P, Keller M, Marubayashi S, Shank K, Rampal R, et al. Improved targeting of JAK2 leads to increased therapeutic efficacy in myeloproliferative neoplasms. Blood 2014;123:2075–83.
5. Yan D, Hutchison RE, Mohi G. Critical requirement for Stat5 in a mouse model of polycythemia vera. Blood 2012;119:3539–49.
6. Chapeau EA, Mandon E, Gill J, Romanet V, Ebel N, Powajbo V, et al. A conditional inducible JAK2V617F transgenic mouse model reveals myeloproliferative disease that is reversible upon switching off transgene expression. PLoS One 2019;14:e0221635.
7. Castagnetti F, Gugliotta G, Breccia M, Stagno F, Iurlo A, Albano F, et al. Long-term outcome of chronic myeloid leukemia patients treated frontline with imatinib. Leukemia 2015;29:1823–31.
8. Harrison CN, Vannucchi AM, Kiladjian JJ, Al-Ali HK, Gisslinger H, Knoops L, et al. Long-term findings from COMFORT-II, a phase 3 study of ruxolitinib vs best available therapy for myelofibrosis. Leukemia 2016;30:1701–7.
9. Deininger M, Radich J, Burn TC, Huber R, Paranagama D, Verstovsek S. The effect of long-term ruxolitinib treatment on JAK2p.V617F allele burden in patients with myelofibrosis. Blood 2015;126:1551–4.
10. Andreoli A, Verger E, Robin M, Raffoux E, Zini JM, Rousselot P, et al. Clinical resistance to ruxolitinib is more frequent in patients without MPN-associated mutations and is rarely due to mutations in the JAK2 kinase drug-binding domain. Blood 2013;122:1591.
11. Brkic S, Meyer SC. Challenges and perspectives for therapeutic targeting of myeloproliferative neoplasms. Hemasphere 2021;5:e516.
12. Koppikar P, Bhagwat N, Kilpivaara O, Manshouri T, Adli M, Hricik T, et al. Heterodimeric JAK-STAT activation as a mechanism of persistence to JAK2 inhibitor therapy. Nature 2012;489:155–9.
13. Stivala S, Codilupi T, Brkic S, Baerenwaldt A, Ghosh N, Hao-Shen H, et al. Targeting compensatory MEK/ERK activation increases JAK inhibitor efficacy in myeloproliferative neoplasms. J Clin Invest 2019;129:1596–611.
14. Jayavelu AK, Schnoder TM, Perner F, Herzog C, Meiler A, Krishnamoorthy G, et al. Splicing factor YBX1 mediates persistence of JAK2-mutated neoplasms. Nature 2020;588:157–63.
15. Anastassiadis K, Fu J, Patsch C, Hu S, Weidlich S, Duerschke K, et al. Dre recombinase, like Cre, is a highly efficient site-specific recombinase in E. coli, mammalian cells and mice. Dis Model Mech 2009;2:508–15.
16. Sauer B. Inducible gene targeting in mice using the Cre/lox system. Methods 1998;14:381–92.
17. Bowman RL, Dunbar AJ, Mishra T, Xiao W, Waarts MR, Fernández Maestre I, et al. Modeling clonal evolution and oncogenic dependency in vivo in the context of hematopoietic transformation. bioRxiv 2022.05.18.492524; doi: https://doi.org/10.1101/2022.05.18.492524.
18. Akada H, Akada S, Hutchison RE, Sakamoto K, Wagner KU, Mohi G. Critical role of Jak2 in the maintenance and function of adult hematopoietic stem cells. Stem Cells 2014;32:1878–89.
19. Grisouard J, Hao-Shen H, Dirnhofer S, Wagner KU, Skoda RC. Selective deletion of Jak2 in adult mouse hematopoietic cells leads to lethal anemia and thrombocytopenia. Haematologica 2014;99:e52–4.
20. Parganas E, Wang D, Stravopodis D, Topham DJ, Marine JC, Teglund S, et al. Jak2 is essential for signaling through a variety of cytokine receptors. Cell 1998;93:385–95.
21. Neubauer H, Cumano A, Muller M, Wu H, Huffstadt U, Pfeffer K. Jak2 deficiency defines an essential developmental checkpoint in definitive hematopoiesis. Cell 1998;93:397–409.
22. Madisen L, Zwingman TA, Sunkin SM, Oh SW, Zariwala HA, Gu H, et al. A robust and high-throughput Cre reporting and characterization system for the whole mouse brain. Nat Neurosci 2010;13:133–40.
23. Poulos MG, Crowley MJP, Gutkin MC, Ramalingam P, Schachterle W, Thomas JL, et al. Vascular platform to define hematopoietic stem cell factors and enhance regenerative hematopoiesis. Stem Cell Rep 2015;5:881–94.
24. Socolovsky M, Nam H, Fleming MD, Haase VH, Brugnara C, Lodish HF. Ineffective erythropoiesis in Stat5a(−/−)5b(−/−) mice due to decreased survival of early erythroblasts. Blood 2001;98:3261–73.
25. Plummer NW, Evsyukova IY, Robertson SD, de Marchena J, Tucker CJ, Jensen P. Expanding the power of recombinase-based labeling to uncover cellular diversity. Development 2015;142:4385–93.
26. Verstovsek S, Kantarjian H, Mesa RA, Pardanani AD, Cortes-Franco J, Thomas DA, et al. Safety and efficacy of INCB018424, a JAK1 and JAK2 inhibitor, in myelofibrosis. N Engl J Med 2010;363:1117–27.
27. Fisher DAC, Miner CA, Engle EK, Hu H, Collins TB, Zhou A, et al. Cytokine production in myelofibrosis exhibits differential responsiveness to JAK-STAT, MAP kinase, and NFkappaB signaling. Leukemia 2019;33:1978–95.
28. Andrews NC, Erdjument-Bromage H, Davidson MB, Tempst P, Orkin SH. Erythroid transcription factor NF-E2 is a haematopoietic-specific basic-leucine zipper protein. Nature 1993;362:722–8.
29. Zhao B, Mei Y, Cao L, Zhang J, Sumagin R, Yang J, et al. Loss of pleckstrin-2 reverts lethality and vascular occlusions in JAK2V617F-positive myeloproliferative neoplasms. J Clin Invest 2018;128:125–40.
30. Krantz SB. Erythropoietin. Blood 1991;77:419–34.
31. Dilip D, Menghrajani K, Melnick A, Elemento O, Levine RL, Glass JL. Single cell ATAC lineage deconvolution reveals overlapping subclones in epigenetically distinct AML samples. Blood 2021;138:2381.
32. Starr R, Willson TA, Viney EM, Murray LJ, Rayner JR, Jenkins BJ, et al. A family of cytokine-inducible inhibitors of signalling. Nature 1997;387:917–21.

33. van der Lugt NM, Domen J, Verhoeven E, Linders K, van der Gulden H, Allen J., et al. Proviral tagging in E mu-myc transgenic mice lacking the Pim-1 proto-oncogene leads to compensatory activation of Pim-2. EMBO J 1995;14:2536–44.
34. Sasaki A, Yasukawa H, Suzuki A, Kamizono S, Syoda T, Kinjyo I, et al. Cytokine-inducible SH2 protein-3 (CIS3/SOCS3) inhibits Janus tyrosine kinase by binding through the N-terminal kinase inhibitory region as well as SH2 domain. Genes Cells 1999;4:339–51.
35. Myers RM, Izzo F, Kottapalli S, Prieto T, Dunbar AJ, Bowman RL, et al. Integrated single-cell genotyping and chromatin accessibility charts JAK2V617F human hematopoietic differentiation. bioRxiv 2022.05.11.491515; doi: https://doi.org/10.1101/2022.05.11.491515.
36. Meyer SC, Keller MD, Chiu S, Koppikar P, Guryanova OA, Rapaport F, et al. CHZ868, a type II JAK2 inhibitor, reverses type I JAK inhibitor persistence and demonstrates efficacy in myeloproliferative neoplasms. Cancer Cell 2015;28:15–28.
37. Karin M. The regulation of AP-1 activity by mitogen-activated protein kinases. J Biol Chem 1995;270:16483–6.
38. Ortmann CA, Kent DG, Nangalia J, Silber Y, Wedge DC, Grinfeld J, et al. Effect of mutation order on myeloproliferative neoplasms. N Engl J Med 2015;372:601–12.
39. Chen E, Schneider RK, Breyfogle LJ, Rosen EA, Poveromo L, Elf S, et al. Distinct effects of concomitant Jak2V617F expression and Tet2 loss in mice promote disease progression in myeloproliferative neoplasms. Blood 2015;125:327–35.
40. Kameda T, Shide K, Yamaji T, Kamiunten A, Sekine M, Taniguchi Y, et al. Loss of TET2 has dual roles in murine myeloproliferative neoplasms: disease sustainer and disease accelerator. Blood 2015;125:304–15.
41. Shepherd MS, Li J, Wilson NK, Oedekoven CA, Li J, Belmonte M, et al. Single-cell approaches identify the molecular network driving malignant hematopoietic stem cell self-renewal. Blood 2018;132:791–803.
42. Moran-Crusio K, Reavie L, Shih A, Abdel-Wahab O, Ndiaye-Lobry D, Lobry C, et al. Tet2 loss leads to increased hematopoietic stem cell self-renewal and myeloid transformation. Cancer Cell 2011;20:11–24.
43. Vasan N, Baselga J, Hyman DM. A view on drug resistance in cancer. Nature 2019;575:299–309.
44. Meyer SC. Mechanisms of resistance to JAK2 inhibitors in myeloproliferative neoplasms. Hematol Oncol Clin North Am 2017;31:627–42.
45. Wu SC, Li LS, Kopp N, Montero J, Chapuy B, Yoda A, et al. Activity of the type II JAK2 inhibitor CHZ868 in B cell acute lymphoblastic leukemia. Cancer Cell 2015;28:29–41.
46. Reis E, Celik H, Marty C, Lei A, Jobe F, Rupar M, et al. Discovery of INCA033989, a monoclonal antibody that selectively antagonizes mutant calreticulin oncogenic function in myeloproliferative neoplasms (MPNs). Blood 2022;140:14–5.
47. Glassman CR, Tsutsumi N, Saxton RA, Lupardus PJ, Jude KM, Garcia KC. Structure of a Janus kinase cytokine receptor complex reveals the basis for dimeric activation. Science 2022;376:163–9.
48. Ruzankina Y, Pinzon-Guzman C, Asare A, Ong T, Pontano L, Cotsarelis G, et al. Deletion of the developmentally essential gene ATR in adult mice leads to age-related phenotypes and stem cell loss. Cell Stem Cell 2007;1:113–26.
49. Corces MR, Buenrostro JD, Wu B, Greenside PG, Chan SM, Koenig JL, et al. Lineage-specific and single-cell chromatin accessibility charts human hematopoiesis and leukemia evolution. Nat Genet 2016;48:1193–203.
50. Granja JM, Corces MR, Pierce SE, Bagdatli ST, Choudhry H, Chang HY, et al. ArchR is a scalable software package for integrative single-cell chromatin accessibility analysis. Nat Genet 2021;53:403–11.
51. Schep AN, Wu B, Buenrostro JD, Greenleaf WJ. chromVAR: inferring transcription-factor-associated accessibility from single-cell epigenomic data. Nat Methods 2017;14:975–8.